Dishevelled enables casein kinase 1–mediated phosphorylation of Frizzled 6 required for cell membrane localization

Received for publication, July 2, 2018, and in revised form, October 5, 2018 Published, Papers in Press, October 11, 2018, DOI 10.1074/jbc.RA118.004656

Katerina Strakova[‡§1], Maria Kowalski-Jahn[§1], Tomas Gybel[‡], Jana Valnohova[§], Vishnu M. Dhople[¶], Jakub Harnos[‡], Ondrej Bernatik[‡], Ranjani Sri Ganji[‡‖], Zbynek Zdrahal[‖], Jan Mulder[**], Cecilia Lindskog[‡‡], Vitezslav Bryja[‡2], and Gunnar Schulte[‡§3]

From the [‡]Laboratory of WNT Signaling, Institute of Experimental Biology, Faculty of Science, Masaryk University, Kotlarska 2, 61137 Brno, Czech Republic, [§]Section for Receptor Biology and Signaling, Department of Physiology and Pharmacology, Karolinska Institutet, Biomedicum (6D), Tomtebodavägen 16, SE-17165 Stockholm, Sweden, [¶]Department of Functional Genomics, Interfaculty Institute for Genetics and Functional Genomics, Ernst Moritz Arndt University of Greifswald, Friedrich-Ludwig-Jahn-Strasse 15, 17487 Greifswald, Germany, [‖]Central European Institute for Technology, Masaryk University, Kamenice 5, 62500 Brno, Czech Republic, [**]Science for Life Laboratory, Department of Neuroscience, Karolinska Institute, Tomtebodavägen 16 17165 Stockholm, Sweden, and [‡‡]Department of Immunology, Genetics and Pathology, Rudbeck Laboratory, Science for Life Laboratory, Uppsala University, Dag Hammarskjölds väg 20, 751 85 Uppsala, Sweden

Edited by Roger J. Colbran

Frizzleds (FZDs) are receptors for secreted lipoglycoproteins of the Wingless/Int-1 (WNT) family, initiating an important signal transduction network in multicellular organisms. FZDs are G protein–coupled receptors (GPCRs), which are well known to be regulated by phosphorylation, leading to specific downstream signaling or receptor desensitization. The role and underlying mechanisms of FZD phosphorylation remain largely unexplored. Here, we investigated the phosphorylation of human FZD_6. Using MS analysis and a phospho-state– and -site–specific antibody, we found that Ser-648, located in the FZD_6 C terminus, is efficiently phosphorylated by casein kinase 1 ε (CK1ε) and that this phosphorylation requires the scaffolding protein Dishevelled (DVL). In an overexpression system, DVL1, -2, and -3 promoted CK1ε-mediated FZD_6 phosphorylation on Ser-648. This DVL activity required an intact DEP domain and FZD-mediated recruitment of this domain to the cell membrane. Substitution of the CK1ε-targeted phosphomotif reduced FZD_6 surface expression, suggesting that Ser-648 phosphorylation controls membrane trafficking of FZD_6. Phospho-Ser-648 FZD_6 immunoreactivity in human fallopian tube epithelium was predominantly apical, associated with cilia in a subset of epithelial cells, compared with the total FZD_6 protein expression, suggesting that FZD_6 phosphorylation contributes to asymmetric localization of receptor function within the cell and to epithelial polarity. Given the key role of FZD_6 in planar cell polarity, our results raise the possibility that asymmetric phosphorylation of FZD_6 rather than asymmetric protein distribution accounts for polarized receptor signaling.

Signal transduction through G protein–coupled receptors (GPCRs)[4] is fine-tuned by phosphorylation (1, 2). Barcoding of receptor function through phosphorylation of intracellular domains of GPCRs is involved in receptor desensitization, recruitment of scaffold proteins such as β-arrestins, functional selectivity, and receptor internalization (3). FZDs functionally interact with the scaffold protein Dishevelled (DVL) to mediate WNT/β-catenin and β-catenin–independent signaling (4, 5). Mammalian DVL exists in three isoforms, DVL1, -2, and -3, and interacts with FZDs, probably in a multimodal fashion involving DVL's DEP domain and the PDZ domain binding the third intracellular loop and the conserved C-terminal KT*XXX*W motif of FZDs, respectively (5–11). Although our understanding of the coupling of Class F receptors to heterotrimeric G proteins is improving (12–15), the role and underlying mechanisms of FZD phosphorylation remain largely obscure. Direct

The work was supported by the Karolinska Institutet, the Swedish Research Council Grants 2013-5708 and 2015-02899, the Science for Life Laboratory, Swedish Cancer Society Grants CAN2014/659 and CAN2017/561), Knut and Alice Wallenberg Foundation Grant KAW2008.0149, Stiftelsen Olle Engkvist Byggmästare Grant 2016/193, Czech Science Foundation Grants 13-32990S and GA17-16680S, Program "KI-MU" Grant CZ.1.07/2.3.00/20.0180 cofinanced by the European Social Fund and the state budget of the Czech Republic, Marie Curie ITN WntsApp Grant 608180, and Deutsche Forschungsgemeinschaft (DFG) German Research Foundation Grant KO 5463/1-1. The authors declare that they have no conflicts of interest with the contents of this article.

This article contains Figs. S1–S5.

The mass spectrometric raw data and spectral libraries associated with this manuscript are available from ProteomeXchange with the accession number PXD011173.

[1] Both authors contributed equally to this work.

[2] To whom correspondence may be addressed: Laboratory of Cellular Communication, Dept. of Experimental Biology, Faculty of Science, Masaryk University, Kotlarska 2, 61137 Brno, Czech Republic. Tel.: 420-549-49-3291; E-mail: bryja@sci.muni.cz.

[3] To whom correspondence may be addressed: Karolinska Institutet, Dept. of Physiology and Pharmacology, Section for Receptor Biology and Signaling, S-171 77 Stockholm, Sweden. Tel.: 46-852487933; E-mail: gunnar.schulte@ki.se.

[4] The abbreviations used are: GPCR, G protein–coupled receptor; CK, casein kinase; DEP, Dishevelled, Egl-10, and pleckstrin domain; DIX, Dishevelled–Axin; DVL, Dishevelled; FZD, Frizzled; GRK, GPCR kinase; PCP, planar cell polarity; WNT, Wingless/Int-1; PKA, cAMP-dependent protein kinase; GSK3, glycogen synthase kinase 3; AP, alkaline phosphatase; KO, knockout; RFP, red fluorescent protein; IP, immunoprecipitation; N-gF, *N*-glycosidase F; FA, formic acid; HPA, Human Protein Atlas; ANOVA, analysis of variance; GAPDH, glyceraldehyde-3-phosphate dehydrogenase.

A

FZD$_6$-496-SKKTCTEWAGFFKRNRKRDPISESRRVLQESCEFFLKHNSKVKHKKKHYKPSSHK
LKVISKSMGTSTGATANHGTSAVAITSHDYLGQETLTEIQTSPETSMREVKADGASTPRLREQDC
GEPASPAASISRLSGEQVDGKGQAGSVSESARSEGRISPKSDITDTGLAQSNNLQVPSSSEPSS
LKGSTSLLVHPVSGVRKEQGGGCHSDT-706

B

	relative peak area of peptides containg indicated phosphorylated amino acid					
ctrl	52,90	94,10	64,70	0,00	5,80	5,80
WNT-3A	29,40	70,50	23,50	47,00	76,40	41,10
WNT-5A	17,60	88,20	35,20	58,80	100,00	82,30
	Ser(P)-592	**Ser(P)-620**	**Ser(P)-629**	**Ser(P)-648**	**Ser(P)-653**	**Ser(P)-656**
	EIQT**S***PETS	GEPA**S***PAAS	ISRL**S***GEQV	ESAR**S***EGRI	EGRI**S***PKSD	ISPK**S***DITD

C

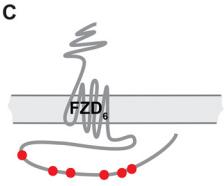

Figure 1. Mass spectrometry analysis of FZD$_6$. *A*, amino acid sequence of the FZD$_6$ C terminus. Putative phosphorylation sites are *underlined* (determined with the MiniMotif Miner software). The KT*XXX*W motif is shown in *orange*. *Black/red* residues correspond to phosphorylation sites detected by LC-MS/MS analysis presented in Fig. 1*B*. *B*, LC-MS/MS data are presented as relative peak areas of all peptides (percentage of maximum) in a sample containing a specific phosphorylated amino acid. Cells lysed for MS were treated with control (*ctrl*), WNT-3A–, or WNT-5A– conditioned medium. *C*, schematic depiction of detected phosphorylation sites (symbolized by *red dots*).

biochemical evidence for phosphorylation of FZDs is sparse, but phosphorylation of FZD$_1$ and FZD$_3$ is involved in negative feedback regulating FZD-mediated signaling along the planar cell polarity pathway, which was found to depend on DVL in the case of FZD$_3$ (16–19).

FZD$_6$, the focus of this study, is closely related to FZD$_3$ (14) and is expressed predominantly in the olfactory epithelium, thyroid and parathyroid glands, lung, and uterus in adult mice (Ref. 20; for an overview of expression in human tissues, see https://www.proteinatlas.org/ENSG00000164930-FZD6/tissue).[5] It has been found amplified in many different forms of cancer, including breast, ovarian, and prostate cancer (21). FZD$_6$ mediates exclusively β-catenin–independent signaling through DVL and as a G$_i$- and G$_q$-coupled receptor (22–26). When mutated, FZD$_6$ can cause nail dysplasia in humans, and knockout mice lacking FZD$_6$ show defects in claw formation, hair patterning, and tissue polarity, phenotypes reflecting dysfunctional planar cell polarity (PCP) signaling (24, 25, 27–30). Polarity of epithelial tissues is defined by asymmetry of epithelial cells perpendicular to the apical-basal axis. WNT/FZD signaling and in particular the closely related FZD$_3$ and FZD$_6$ are crucial for the polarity and PCP signaling in cells and tissues (24, 25, 27, 31). However, it remains a conundrum how asymmetry is achieved by a protein that does not necessarily show polarized cellular distribution (32).

In the present study, we investigated the mechanisms and role of C-terminal FZD$_6$ phosphorylation. Our results identify serine 648 (Ser-648) as a CK1ϵ target site, and we propose a mechanism where DVL and CK1ϵ cooperate to achieve FZD$_6$ phosphorylation at the plasma membrane. The development of a phospho-Ser-648–selective polyclonal FZD$_6$ antibody enabled us to depict polarization of phosphorylated FZD$_6$ in epithelial cells of the human fallopian tube, suggesting that phosphorylation of FZD$_6$ rather than asymmetric localization could code for polarized signaling.

Results

Mass spectrometry analysis of FZD$_6$ phosphorylation

The C terminus of human FZD$_6$ is 211 amino acids long and contains more than 50 phosphorylatable amino acids (Fig. 1*A*). Previous analysis with the MiniMotif Miner predicted the presence of two cAMP-dependent protein kinase (PKA), eight Ca^{2+}-dependent protein kinase, eight casein kinase 1 (CK1), seven casein kinase 2 (CK2), one Ca^{2+}/calmodulin-dependent protein kinase II, five ribosomal S6 kinase, one extracellular signal-regulated kinase 1/2, seven glycogen synthase kinase 3 (GSK3), one polo-like kinase, and one epidermal growth factor receptor sites (33). To assess FZD$_6$ phosphorylation experimentally, we used MS. HEK293 cells expressing FZD$_6$-GFP were treated with either control, WNT-3A–, or WNT-5A– containing conditioned medium for 30 min and processed for LC-MS/MS analysis. Six phosphorylated serine residues were detected in the C terminus of FZD$_6$ (Fig. 1, *B* and *C*). Despite stimulation with conditioned medium, the detected phosphorylation events were rare compared with the amount of predicted kinase sites and phosphorylatable residues in FZD$_6$. In total, phosphorylation in six positions was detected on Ser-592, Ser-620, Ser-629, Ser-648, Ser-653, and Ser-656 (Fig. 1*C*). Although Ser-592, Ser-620, and Ser-629 appeared to be constitutively phosphorylated and we could detect tendencies for agonist-induced phosphorylation in Ser-648, Ser-653, and Ser-656, the total number of detected peptides did not allow firm conclusions on WNT-induced changes.

FZD$_6$ phosphorylation at Ser-648 is detectable using a phospho-specific antibody

Despite our initial interest in several phosphorylatable residues in the C terminus of FZD$_6$, we became particularly interested in the phosphorylation of Ser-648 because we were able to raise a phospho-specific antibody against this residue (SESARpS*EGRISP peptide where pS* is Ser(P)-648; Fig. 2*A*). The anti-Ser(P)-648 rabbit polyclonal antibody displayed a weak signal when detecting overexpressed FZD$_6$ (V5-FZD$_6$-mCherry; Fig. 2*B*) in HEK293 cells; however, the signal was specific as it did not detect the FZD$_6$-S648A mutant where serine 648 was mutated to alanine (Fig. 2*C*). The antibody is phospho-selective because alkaline phosphatase (AP) treatment of the lysate abolished the signal (Fig. 2*D*). Concurrently, we validated the FZD$_6$-S648A mutant with regard to its membrane localization (Fig. 2*E*) and glycosylation (Fig. 2*F*) compared with WT FZD$_6$, indicating that the point mutation does not affect overall maturation of the receptor protein. In contrast, cell ELISA–based assessment of receptor surface expression

[5] Please note that the JBC is not responsible for the long-term archiving and maintenance of this site or any other third party-hosted site.

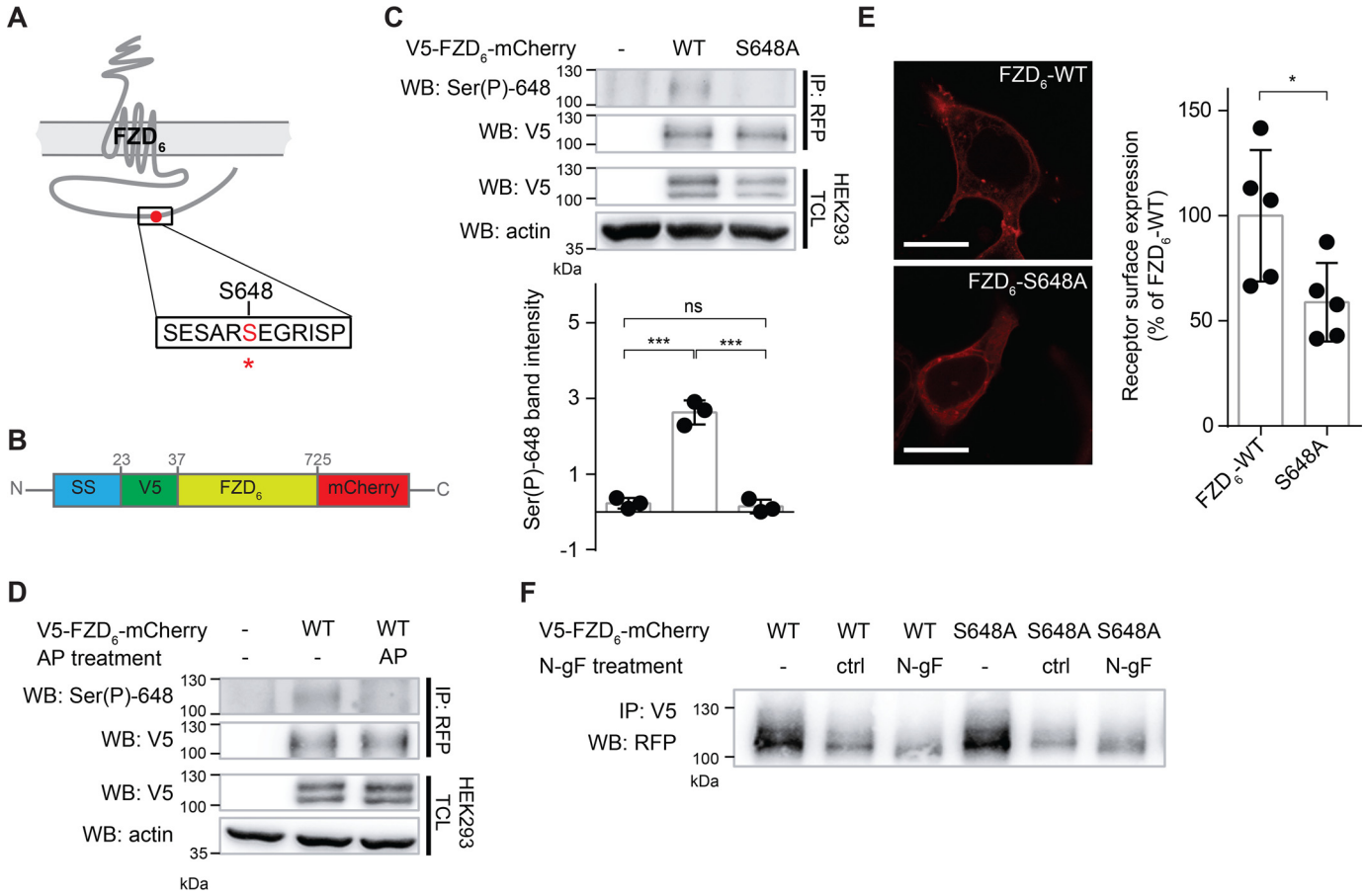

Figure 2. FZD$_6$ is phosphorylated on Ser-648. *A*, schematic depiction of the phosphorylated (*red*, *asterisk*) human FZD$_6$-based (UniProt ID O60353) peptide used for raising a phospho-specific polyclonal (rabbit) antibody (anti-Ser(P)-648 FZD$_6$). *B*, schematic depiction of the WT FZD$_6$ construct consisting of signal sequence (*SS*), V5 tag, FZD$_6$, and mCherry. *C*, HEK293 cells transfected with pcDNA3.1 (control), WT V5-FZD$_6$-mCherry, or V5-FZD$_6$-S648A-mCherry were lysed, and immunoprecipitation was performed using an anti-RFP (mCherry) antibody. Precipitate (*IP*) was probed with anti-V5 and the Ser(P)-648 FZD$_6$ antibodies. Total cell lysate (*TCL*) was probed with anti-V5 and anti-β-actin as a loading control. The density of Ser(P)-648–stained bands, measured using ImageJ, was normalized by dividing the value by the average of the whole experiment. Data are presented as a scatter plot; *bars* represent mean and *error bars* represent S.D. of three individual experiments. Selected results of the multiple comparison analysis of all data are presented. Results were analyzed with one-way ANOVA and Tukey's multiple comparisons post hoc test. Significance levels are given as *** ($p < 0.001$) and *ns* (not significant). *D*, cell lysates were treated with AP. *E*, subcellular distribution of WT V5-FZD$_6$-mCherry or V5-FZD$_6$-S648A-mCherry was analyzed by confocal microscopy in living HEK293 cells. *Scale bars*, 10 μm. Cell ELISA was used to quantify surface expression of WT V5-FZD$_6$-mCherry or V5-FZD$_6$-S648A-mCherry using an antibody against the N-terminal V5 tag. Data are presented as a scatter plot; *bars* represent mean and *error bars* represent S.D. of five individual experiments performed in triplicates. Background fluorescence detected in pcDNA-transfected HEK293 cells was subtracted from all data, and mean values were normalized to WT FZD$_6$ surface expression. Significance levels are given as * ($p < 0.05$). *F*, for detection of *N*-linked glycosylation, immunoprecipitates were treated with N-gF, analyzed by PAGE, and probed with anti-RFP. HEK293 lysates expressing WT V5-FZD$_6$-mCheery or V5-FZD$_6$-S648A-mCherry were divided into three equal parts, and FZD$_6$ was pulled down using an anti-V5 antibody. The first sample was left untreated (−), the second was subjected to the deglycosylation treatment but without the enzyme (*ctrl*), and the third sample was subjected to the deglycosylation treatment including the enzyme (*N-gF*). *WB*, Western blot.

indicated that significantly lower levels of FZD$_6$-S648A compared with WT FZD$_6$ are present in the plasma membrane (Fig. 2*E*).

FZD$_6$ Ser-648 is phosphorylated in a CK1ϵ-dependent manner

In silico phospho-prediction analysis of FZD$_6$ using the Mini-Motif Miner software (34) suggested that Ser-648 provides a consensus site for casein kinase 1 (Fig. 3*A*). Furthermore, Ser-645 was predicted to serve as a priming site enabling CK1-dependent phosphorylation of Ser-648.

We therefore decided to test CK1ϵ as a candidate kinase and coexpressed it with FZD$_6$. As shown in Fig. 3*B*, coexpression of CK1ϵ leads to a substantial increase in the Ser(P)-648 FZD$_6$ signal accompanied by increased binding of CK1ϵ to FZD$_6$. To verify that the Ser-648 phosphorylation depends on CK1ϵ activity, we treated the cells with the CK1δ/ϵ-selective inhibitor PF670462, which abrogated the Ser(P)-648 signal. Also, the Ser(P)-648 signal was sensitive to AP treatment of the lysates, and the S648A mutant was not phosphorylated upon CK1ϵ coexpression, which further confirmed the specificity of the detected Ser(P)-648 signal.

To explore the priming properties of Ser-645, we created two additional mutants: Ser-645 was mutated to either alanine (S645A) to disable phosphorylation of Ser-645 or to glutamate (S645E), which was intended to mimic the priming phosphorylation event. Both mutants were localized in the membrane, albeit with slightly lower surface expression compared with the WT receptor (Fig. 3*C*). When coexpressed with CK1ϵ, the S645A mutant did not exhibit a Ser(P)-648 signal compared with the WT receptor (Fig. 3*D*). In contrast, when S645E was coexpressed with CK1ϵ, the observed Ser(P)-648 signal was stronger than that of the WT FZD$_6$. Overexpressing S645E on

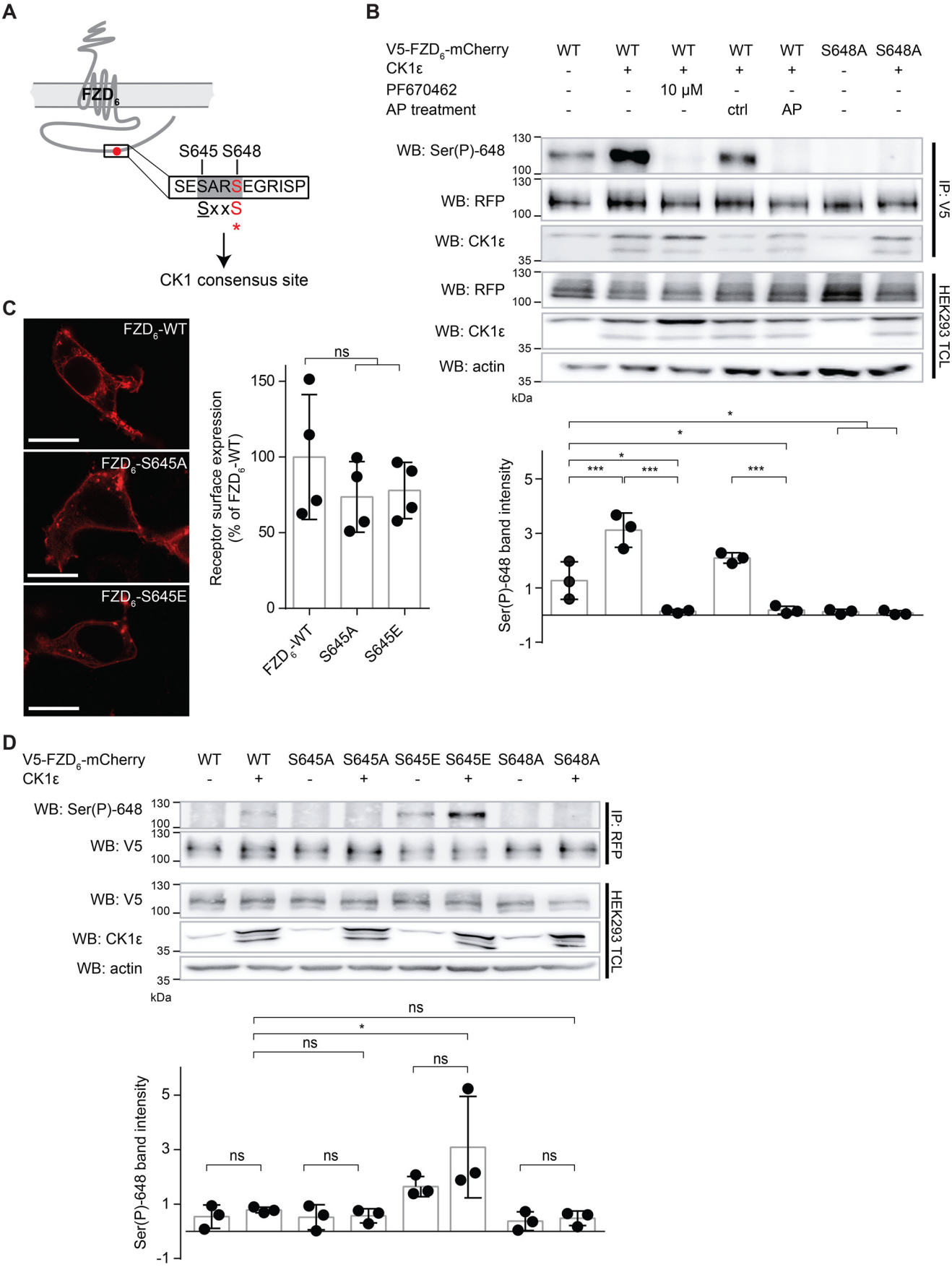
A
FZD6
S645 S648
SESARSEGRISP
SxxS
*
CK1 consensus site
B
V5-FZD6-mCherry WT WT WT WT WT S648A S648A
CK1ε - + + + + - +
PF670462 - - 10 μM - - - -
AP treatment - - - ctrl AP - -
WB: Ser(P)-648
WB: RFP
WB: CK1ε
WB: RFP
WB: CK1ε
WB: actin
kDa
IP: V5
HEK293 TCL
Ser(P)-648 band intensity
C
FZD6-WT
FZD6-S645A
FZD6-S645E
Receptor surface expression (% of FZD6-WT)
ns
FZD6-WT
S645A
S645E
D
V5-FZD6-mCherry WT WT S645A S645A S645E S645E S648A S648A
CK1ε - + - + - + - +
WB: Ser(P)-648
WB: V5
WB: V5
WB: CK1ε
WB: actin
kDa
IP: RFP
HEK293 TCL
Ser(P)-648 band intensity
ns

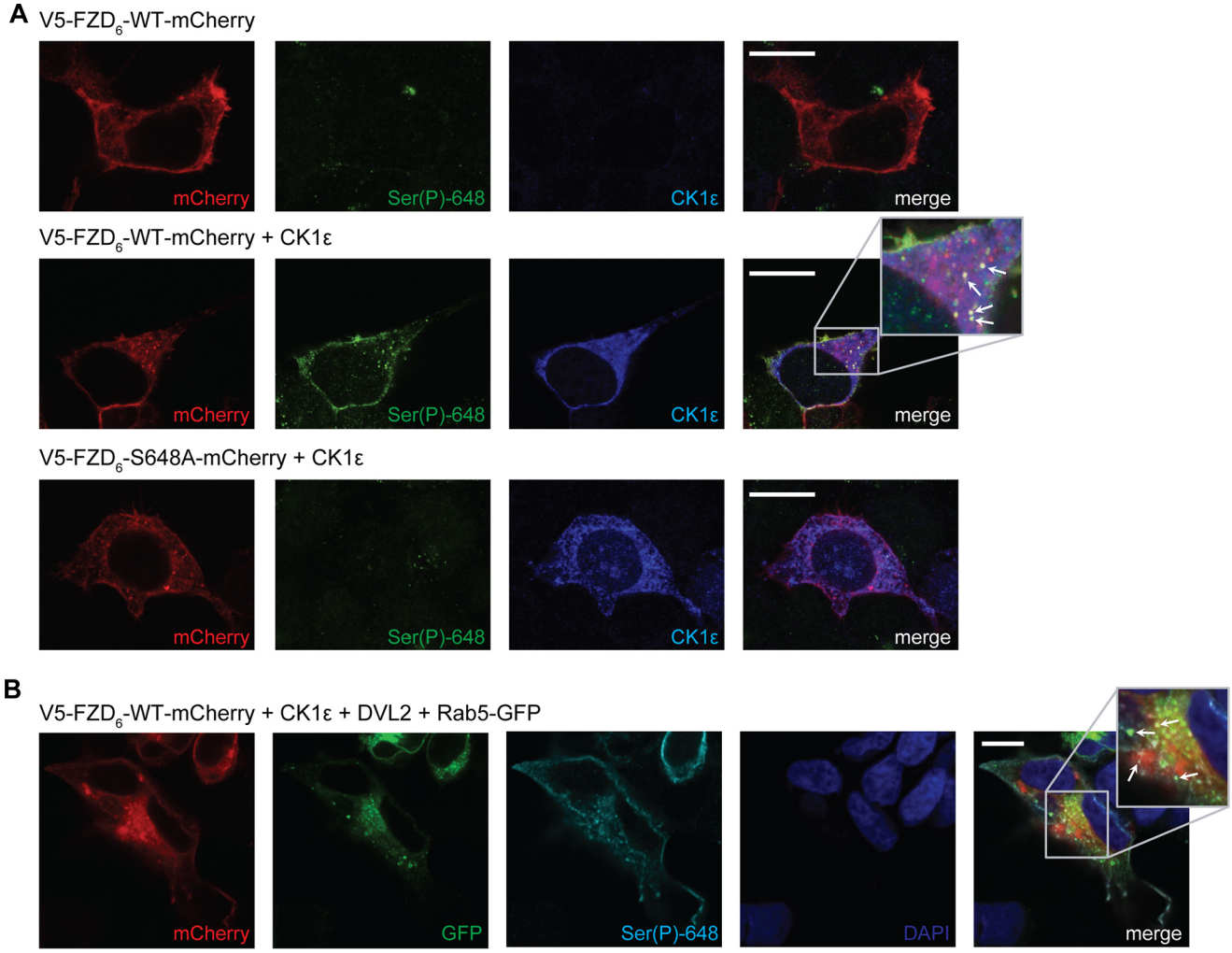

Figure 4. Phosphorylated FZD$_6$ is predominantly localized in the plasma membrane and processed through the endosomal pathway. *A*, HEK293 cells transfected with WT V5-FZD$_6$-mCherry or V5-FZD$_6$-S648A-mCherry in combination with CK1ϵ were fixed in 4% paraformaldehyde, stained with anti-Ser(P)-648 FZD$_6$ and anti-CK1ϵ, and visualized with a confocal microscope. *Arrows* point to Ser(P)-648 FZD$_6$ detection in intracellular puncta. *Scale bars*, 10 μm. *B*, HEK293 cells cotransfected with WT V5-FZD$_6$-mCherry, CK1ϵ, DVL2, and Rab5-GFP. Rab5-GFP serves as an early endosome marker. The cells were fixed in 4% paraformaldehyde, stained with anti-Ser(P)-648 and DAPI, and visualized with a confocal microscope. *Arrows* point to Ser(P)-648 FZD$_6$– and Rab5-GFP–positive endosomes. *Scale bar*, 10 μm.

its own led to a Ser(P)-648 signal comparable with the WT receptor in the presence of overexpressed CK1ϵ. These findings suggest that Ser-645 indeed serves as a priming site for CK1ϵ.

The anti-Ser(P)-648 antibody enabled us to visualize phosphorylated FZD$_6$ in relation to the FZD$_6$-mCherry signal using indirect immunofluorescence in HEK293 cells coexpressing CK1ϵ and FZD$_6$. FZD$_6$-mCherry is widely distributed in the cell with a distinct fraction in the plasma membrane, similar to what we have reported before for this or similar constructs (22, 23, 30, 35). However, the WT FZD$_6$ phosphorylated at Ser-648 was predominantly present at the plasma membrane (Fig. 4*A*). In addition, phosphorylated FZD$_6$ was detectable in intracellular puncta, most likely early endosomes or lysosomes. To confirm the localization of the phosphorylated FZD$_6$ to the endosomal pathway, which would be in agreement with previous data (30), we used the anti-Ser(P)-648 antibody in cells coex-

Figure 3. FZD$_6$ Ser-648 is phosphorylated in a CK1ϵ-dependent manner. *A*, schematic depiction of a CK1 consensus site matching the sequence of human FZD$_6$ (*gray background*). Ser-648, the phospho-acceptor serine in the CK1 consensus site, is highlighted in *red* and marked with an *asterisk*. The predicted CK1 priming site Ser-645 is *underlined*. *B*, HEK293 cells transfected with WT V5-FZD$_6$-mCherry or V5-FZD$_6$-S648A-mCherry in combination with CK1ϵ were treated with the CK1 inhibitor PF670462 (10 μM; overnight). Cells were lysed, and immunoprecipitation was performed using an anti-V5 antibody. Precipitate (*IP*) was probed with the anti-Ser(P)-648 FZD$_6$, anti-CK1ϵ, and anti-RFP (mCherry) antibodies. To verify phosphate specificity of the anti-Ser(P)-648 antibody, lysates were treated with AP. The total cell lysate (*TCL*) was probed with anti-RFP and anti-CK1ϵ. Anti-β-actin served as a loading control. *C*, living HEK293 cells are shown expressing either WT V5-FZD$_6$-mCherry, V5-FZD$_6$-S645A-mCherry, or V5-FZD$_6$-S645E-mCherry. *Scale bars*, 10 μm. Cell ELISA was performed to quantify the construct's surface expression compared with the WT V5-FZD$_6$-mCherry construct using an antibody against the N-terminal V5 tag. Data are presented as a scatter plot; *bars* represent mean and *error bars* represent S.D. of four individual experiments performed in triplicates. Background fluorescence detected in pcDNA-transfected HEK293 cells was subtracted, and mean values were normalized to FZD$_6$ surface expression. *ns*, not significant. *D*, anti-RFP immunoprecipitation was done as in Fig. 3*B*. *B* and *D*, the density of Ser(P)-648–stained bands, measured using ImageJ, was normalized by dividing the value by the average of the whole experiment. Data are presented as a scatter plot; *bars* represent mean and *error bars* represent S.D. of three individual experiments. Selected results of the multiple comparison analysis of all data are presented. Results were analyzed with one-way ANOVA and Tukey's multiple comparisons post hoc test. Significance levels are given as * ($p < 0.05$), *** ($p < 0.001$), and *ns* (not significant). *WB*, Western blot; *ctrl*, control.

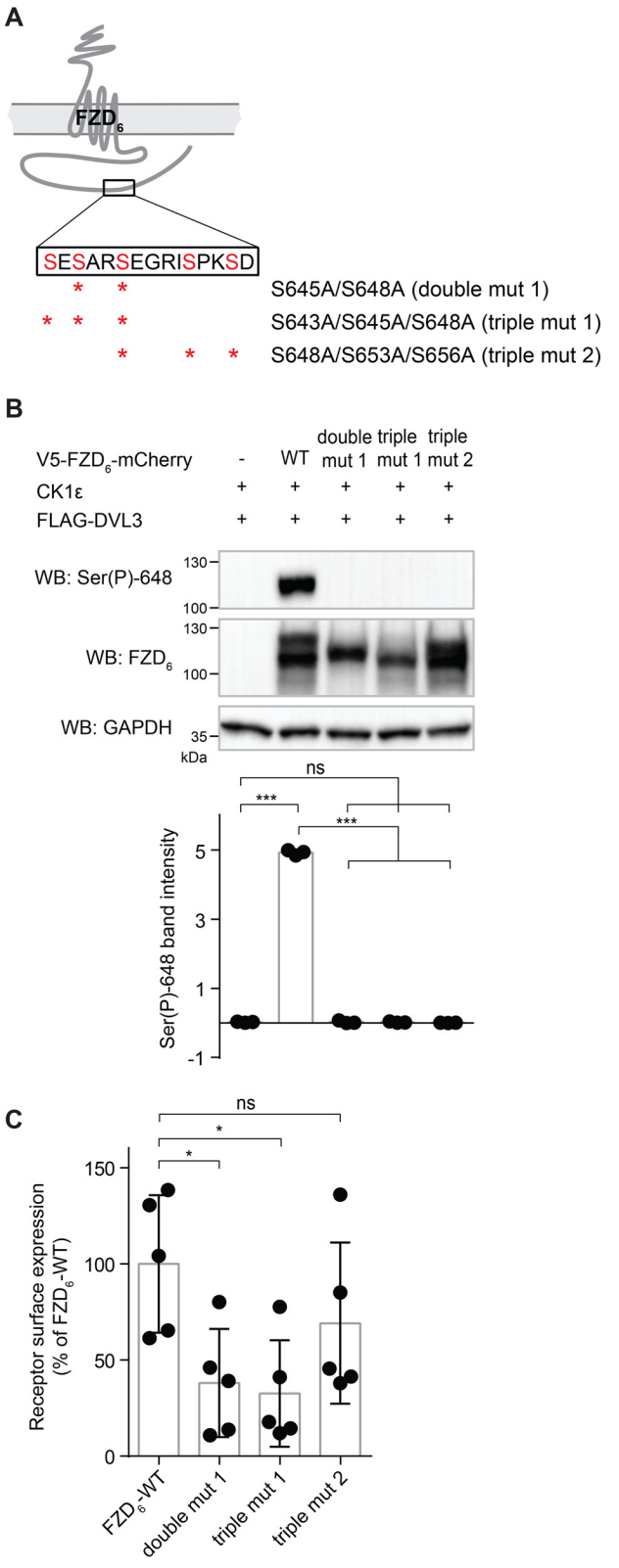

Figure 5. Characterization of the phosphorylatable serine motif by the help of Ser double and triple mutants. *A*, schematic depiction of Ser to Ala mutants, including Ser-648 and adjacent Ser residues. *B*, HEK293 cells cotransfected with pcDNA3.1 (control), WT V5-FZD$_6$-mCherry, V5-FZD$_6$-S645A/S648A-mCherry (*double mut 1*), V5-FZD$_6$-S643A/S645A/S648A-mCherry (*triple mut 1*), or V5-FZD$_6$-S648A/S653A/S656A-mCherry (*triple mut 2*); FLAG-DVL3; and CK1ϵ were lysed and analyzed by immunoblotting using anti-Ser(P)-648 and anti-FZD$_6$ antibodies. Anti-GAPDH served as a loading control. The density of Ser(P)-648–stained bands, measured using ImageJ, was normalized by dividing each value by the average of the whole experiment. Data are presented as a scatter plot; *bars* represent mean and *error bars* represent S.D. of three individual experiments. Selected results of the multiple comparison analysis of all data are presented. Results were analyzed with one-way ANOVA and Tukey's multiple comparisons post hoc test. Significance levels are given as *** ($p < 0.001$) and *ns* (not significant). *C*, receptor surface expression of HEK293 cells transiently transfected with pcDNA3.1, WT V5-FZD$_6$-mCherry, V5-FZD$_6$-S645A/S648A-mCherry (*double mut 1*), V5-FZD$_6$-S643A/S645A/S648A-mCherry (*triple mut 1*), or V5-FZD$_6$-S648A/S653A/S656A-mCherry (*triple mut 2*) was quantified by cell ELISA using an antibody against the N-terminal V5 tag. Data are presented as a scatter plot; *bars* represent mean and *error bars* represent S.D. of five individual experiments performed in triplicates. Background fluorescence detected in pcDNA-transfected HEK293 cells was subtracted from all data, and mean values were normalized to WT FZD$_6$ surface expression. Significance levels are given as * ($p < 0.05$) and *ns* (not significant). *WB*, Western blot.

pressing CK1ϵ, DVL, V5-FZD$_6$-mCherry, and GFP-tagged Rab5, a marker for early endosomes. Under these conditions, which allow efficient FZD$_6$ phosphorylation at Ser-648, we observed punctate, intracellular structures that were positive for the FZD$_6$ protein (mCherry), Ser(P)-648 (anti-Ser(P)-648 FZD$_6$ antibody), and the endosomal marker Rab5-GFP (Fig. 4*B*).

As shown above, point mutations of phosphorylatable amino acids revealed phospho-specificity of the antibody and target-selective phosphorylation by CK1. However, we only observed slight reduction in surface expression of these receptor constructs (Fig. 3*C*). Based on a recent publication reporting on phosphorylation codes spanning three phosphorylatable residues mediating arrestin–GPCR interaction, we reasoned that functional consequences could become more apparent when mutating larger phosphorylation motifs (36). To evoke more serious malfunction, we therefore decided to systematically mutate the phosphorylatable motif, targeting several residues, including the Ser-648 and adjacent serines. We created two triple mutants, S643A/S645A/S648A and S648A/S653A/S656A, which were expressed well on the protein level. The S643A/S645A/S648A mutant, however, showed dramatically reduced surface expression (Fig. 5, *A–C*). This effect was phenocopied by the S645A/S648A double mutant, which is deficient in the CK1ϵ priming and target site.

DVL is required to induce phosphorylation of FZD$_6$ in response to CK1ϵ

CK1ϵ is a serine/threonine kinase with well defined function in WNT signaling. Its primary substrates in this pathway are the DVL proteins that strongly interact with CK1 and are phosphorylated in response to WNT proteins. Because DVL interacts with FZD$_6$ and is phosphorylated and regulated by CK1ϵ (22, 37–39), we asked whether DVL is required for phosphorylation of FZD$_6$ at Ser-648. We overexpressed FZD$_6$ and CK1ϵ in HEK293 cells depleted of all DVL proteins by CRISPR/Cas9 (DVL-KO-HEK293 cells; Ref. 40) and observed no signal for Ser(P)-648 (Fig. 6*A*). Reconstitution with either of the three DVL isoforms rescued the Ser(P)-648 signal and resulted in an electrophoretic up-shift of FZD$_6$ when FZD$_6$ and CK1ϵ were coexpressed.

Furthermore, we wanted to find out whether the posttranslational modification of FZD$_6$ induced by overexpression of DVL and resulting in the electrophoretic mobility shift of FZD$_6$ is evoked by receptor phosphorylation and/or *N*-glycosylation.

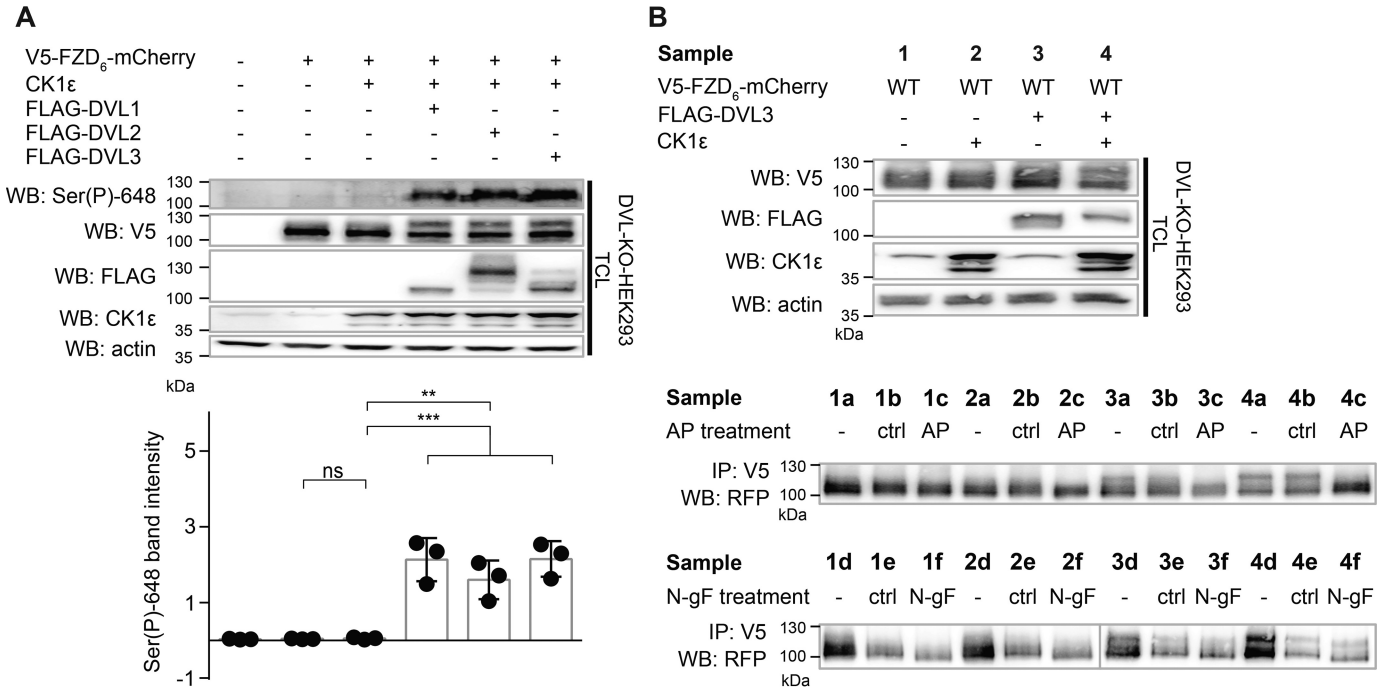

Figure 6. DVL promotes CK1ϵ-dependent FZD$_6$ phosphorylation. *A*, HEK293 cells lacking DVL1, -2, and -3 (DVL-KO-HEK293 (40)) were transfected with WT V5-FZD$_6$-mCherry and combinations of CK1ϵ with FLAG-DVL1, -DVL2, and -DVL3. Lysates were analyzed by immunoblotting and probed for Ser(P)-648, V5, FLAG, CK1ϵ, and β-actin as a loading control. The density of Ser(P)-648–stained bands, measured using ImageJ, was normalized by dividing each value by the average of the whole experiment. Data are presented as a scatter plot; *bars* represent mean and *error bars* represent S.D. of three individual experiments. Selected results of the multiple comparison analysis of all data are presented. Results were analyzed with one-way ANOVA and Tukey's multiple comparisons post hoc test. Significance levels are given as ** ($p < 0.01$), *** ($p < 0.001$), and *ns* (not significant). *B*, DVL-KO-HEK293 lysates with overexpressed WT V5-FZD$_6$-mCherry and combinations of CK1ϵ with FLAG-DVL3. Samples (numbered *1–4* according to the figure annotation) were divided into six equal fractions (denoted *a–f*), and V5-FZD$_6$-mCherry was precipitated with an anti-V5 antibody in each fraction. Post-IP, fractions *a*/*d* were left untreated (−), fractions *b*/*e* were subjected to the dephosphorylation/deglycosylation treatment devoid of enzyme (*ctrl*), and fractions *c*/*f* were subjected to the dephosphorylation/deglycosylation treatment, including either AP or N-gF. Immunoblots show abundance of proteins in the pulldown (*IP*) or total cell lysate (*TCL*) detected by anti-V5, anti-FLAG, anti-CK1ϵ, and anti-RFP (mCherry) antibodies. Anti-β-actin served as a loading control. *WB*, Western blot.

Therefore, we overexpressed FZD$_6$ alone or together with CK1ϵ and DVL3 followed by either enzymatic dephosphorylation or deglycosylation. Only treatment with alkaline phosphatase resulted in a decrease of the FZD$_6$ band at lower mobility, whereas treatment with *N*-glycosidase F did not (Fig. 6*B*), confirming the importance of FZD$_6$ phosphorylation for the electrophoretic mobility shift of the receptor protein. Similar data were obtained when reconstituting the DVL-KO cells with FLAG-DVL1 or FLAG-DVL2 in combination with V5-FZD$_6$-mCherry and CK1ε and subsequent treatment of the lysate with AP (Fig. S1).

To investigate whether Ser-648 is phosphorylated as part of the DVL-induced FZD$_6$ phosphorylation, the same two samples were loaded in parallel and analyzed by antibodies against RFP and Ser(P)-648 (Fig. 7*A*). We observed that the DVL-induced electrophoretic mobility shift of FZD$_6$ (marked by a *filled arrowhead*) corresponds roughly to the Ser(P)-648 signal (marked by *two stars*), and both these signals migrate at ~20 kDa higher molecular mass ("hyperphosphorylated" FZD$_6$) compared with the two species of FZD$_6$ (glycosylated and unglycosylated; marked by *open arrowheads*) detected by the anti-RFP antibody. In addition, we observed a weaker and faster migrating Ser(P)-648 FZD$_6$ band (marked by *one star*), which could represent unspecific binding of anti-Ser(P)-648 to unphosphorylated FZD$_6$. This band was only observed upon very high overexpression of the receptor and was insensitive to AP treatment (Fig. S2).

We confirmed that the DVL-dependent shift of FZD$_6$ is detectable in the WT HEK293 cells upon DVL overexpression (Fig. 7, *A* and *B*). In Fig. 7*B*, we show that overexpressing both CK1ϵ and DVL3 had an additive effect on the amount of Ser(P)-648 and the shifted form of FZD$_6$ compared with expression of CK1ϵ or DVL3 alone. Also, the DVL-induced shift of FZD$_6$ and phosphorylation of Ser-648 were to a great extent (although not exclusively) dependent on the activity of CK1ϵ (Fig. 7, *A* and *B*). Thus, CK1ϵ is crucial for phosphorylation of FZD$_6$ in the presence of DVL even though we cannot exclude that other kinases participate in this process.

The DVL-dependent electrophoretic mobility shift of FZD is not limited to FZD$_6$. We were able to detect a DVL-dependent electrophoretic mobility up-shift of FZD$_4$ when coexpressed with DVL2 (11). In DVL-KO-HEK293 cells, a DVL2-dependent shift of FZD$_4$ was observed when WT receptor was expressed. However, when FZD$_4$-Y250F, a mutant that is impaired in DVL2 binding (11), was expressed, the DVL2-dependent shift was reduced (Fig. S3), suggesting that FZD–DVL interaction and receptor phosphorylation go hand in hand. Furthermore, a similar DVL-induced, phosphorylation-dependent electrophoretic mobility shift was reported for FZD$_3$ (17, 19).

FZD$_6$ is phosphorylated in a GRK-dependent manner

The findings that DVL-dependent FZD$_6$ phosphorylation was not fully inhibited by pharmacologically blocking CK1δ/ϵ and that FZD$_4$, which lacks a residue homologous to Ser-648 in FZD$_6$, was also shifted by DVL raises the question whether there are other kinases involved in FZD$_6$ phosphorylation. To

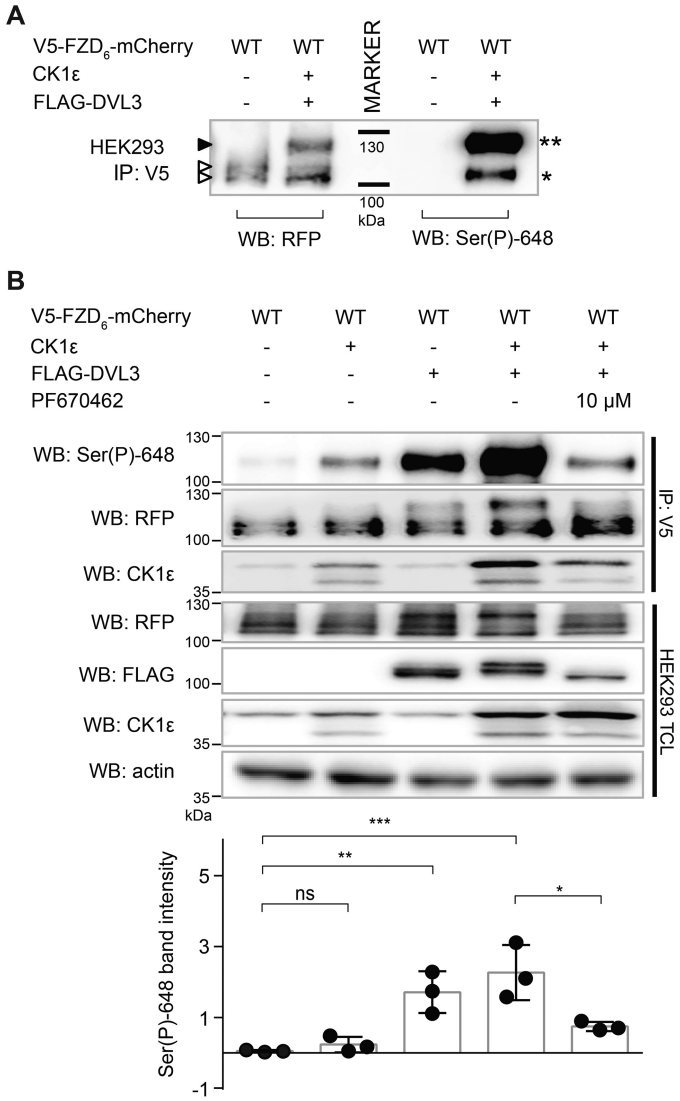

Figure 7. DVL induces phosphorylation of FZD$_6$. *A*, HEK293 cells were transfected with WT V5-FZD$_6$-mCherry in the absence or presence of CK1ϵ and FLAG-DVL3. V5-FZD$_6$-mCherry was precipitated using an anti-V5 antibody, and samples were probed with either anti-Ser(P)-648 FZD$_6$ or anti-RFP (mCherry) antibody. The same two samples were loaded twice, separated by a marker lane. The *filled arrowhead* depicts hypershifted species of V5-FZD$_6$-mCherry. *Open arrowheads* indicate glycosylated (*upper*) and unglycosylated (*lower*) forms of V5-FZD$_6$-mCherry. ** marks the phosphorylated receptor positive for Ser(P)-648 FZD$_6$. * depicts either an unspecific signal from anti-Ser(P)-648 antibody (unphosphorylated FZD$_6$) or a weakly phosphorylated species. *B*, HEK293 cells overexpressing V5-FZD$_6$-mCherry were cotransfected with combinations of CK1ϵ and FLAG-DVL3 and treated with the CK1ϵ inhibitor PF670462 (10 μM; overnight), and V5-FZD$_6$-mCherry was precipitated using an anti-V5 antibody. Immunoblots show abundance of proteins in the pulldown (*IP*) or total cell lysate (*TCL*) detected by anti-Ser(P)-648, anti-RFP, anti-CK1ϵ, and anti-FLAG antibodies. Anti-β-actin served as a loading control. The density of Ser(P)-648–stained bands, measured using ImageJ, was normalized by dividing each value by the average of the whole experiment. Data are presented as a scatter plot; *bars* represent mean and *error bars* represent S.D. of three individual experiments. Selected results of the multiple comparison analysis of all data are presented. Results were analyzed with one-way ANOVA and Tukey's multiple comparisons post hoc test. Significance levels are given as * ($p < 0.05$), ** ($p < 0.01$), *** ($p < 0.001$), and *ns* (not significant). *WB*, Western blot.

investigate other candidate kinases potentially mediating the DVL-induced phosphorylation of FZD$_6$, we used inhibitors of GSK3 (CHIR99021), PKA (H89), or GRK2 (paroxetine) (Fig. 8*A*). The CK1δ/ϵ inhibitor PF670462 was used as a positive control. Although inhibition of PKA or GSK3 did not reduce the Ser(P)-648 FZD$_6$ signal, paroxetine reduced Ser(P)-648 to a similar extent as PF670462, pinpointing GRK2 as an FZD$_6$ kinase. To investigate the role of GRK2 and the paroxetine-insensitive GRK5 as FZD$_6$ kinases in more detail, we overexpressed either CK1ϵ, GRK2, or GRK5 with FZD$_6$ in HEK293 cells endogenously expressing DVL. As shown in Fig. 8*B*, both GRK2 and GRK5 induced FZD$_6$ phosphorylation effectively under these conditions.

To investigate the relationship between the CK1-induced and DVL-dependent Ser-648 FZD$_6$ phosphorylation and membranous expression of FZD$_6$, we used a previously characterized nail dysplasia mutant of this receptor, the FZD$_6$-R511C mutant (22, 30). The R511C mutant results in decreased surface expression and prominent localization of FZD$_6$-R511C to the endosomal/lysosomal pathway (30). The comparison of WT FZD$_6$ and FZD$_6$-R511C in the absence and presence of coexpressed CK1ϵ and DVL3 indicates that WT FZD$_6$ is more efficiently phosphorylated than FZD$_6$-R511C at similar total expression levels of the two receptor constructs (Fig. 8*C*).

The DEP domain of DVL is required for Ser-648 phosphorylation and the shift of FZD$_6$

To better understand underlying mechanisms of DVL-mediated phosphorylation of FZD$_6$, we overexpressed FZD$_6$ in DVL-KO-HEK293 cells in combination with either DVL3 or various deletion or point mutants of DVL3 (Fig. 9*A*). The DVL3 ΔDIX mutant is missing the N-terminal DIX domain important for multimerization and β-catenin signaling (41, 42). DVL3 ΔCterm lacks the very C terminus of DVL. Phosphorylation of this region disrupts the signalosomes observed as puncta and is inhibitory for β-catenin–dependent signaling (38). DVL3 Δ(DEP+C) is missing the DEP domain in addition to missing the C terminus, whereas DVL3 DEP represents the DEP domain of DVL3. In the DVL3-K435M mutant, the binding interface of FZD–DVL is disrupted, and thus, this mutant is not recruited to the membrane by FZD (43, 44).

The DIX domain and the C terminus of DVL are dispensable for the induction of both Ser(P)-648 and the electrophoretic mobility shift of FZD$_6$ (Fig. 9, *B* and *C*). However, deleting the C terminus and the DEP domain abolished the effects on FZD$_6$ (Fig. 9*D*). In contrast, overexpression of the DEP domain of DVL3 was neither sufficient to induce Ser(P)-648 nor the shift of FZD$_6$ (Fig. 9*E*), indicating that the DEP domain is required, but not sufficient, to induce Ser(P)-648 and the FZD$_6$ shift. It should be noted, however, that both DVL3 Δ(DEP+C) and the minimal DVL3 DEP displayed lower expression compared with the WT DVL3. The DVL3-K435M mutant neither induced Ser(P)-648 nor the shift of FZD$_6$ (Fig. 9*F*), consistent with the importance of the DEP domain found in Fig. 9*D* and indicating that the ability of DVL to bind FZD is crucial for its activity toward FZD phosphorylation.

Furthermore, we asked which properties of the DVL DEP domain were required for induction of Ser(P)-648 and the FZD$_6$ shift. Several mutants of the DVL1 DEP domain (described in the table in Fig. 10*A* and validated by Paclikova *et al.* (45)) were used. Instead of WT DVL3 as in Fig. 9, we used DVL1(1–502), a mutant of DVL1 lacking the C terminus, as a positive control for Fig. 10. All the other DVL1 mutants were created in the background of the DVL1(1–502) mutant. In Fig. 10*B*, we show that the K438M mutation in DVL1 (corresponding to K435M in

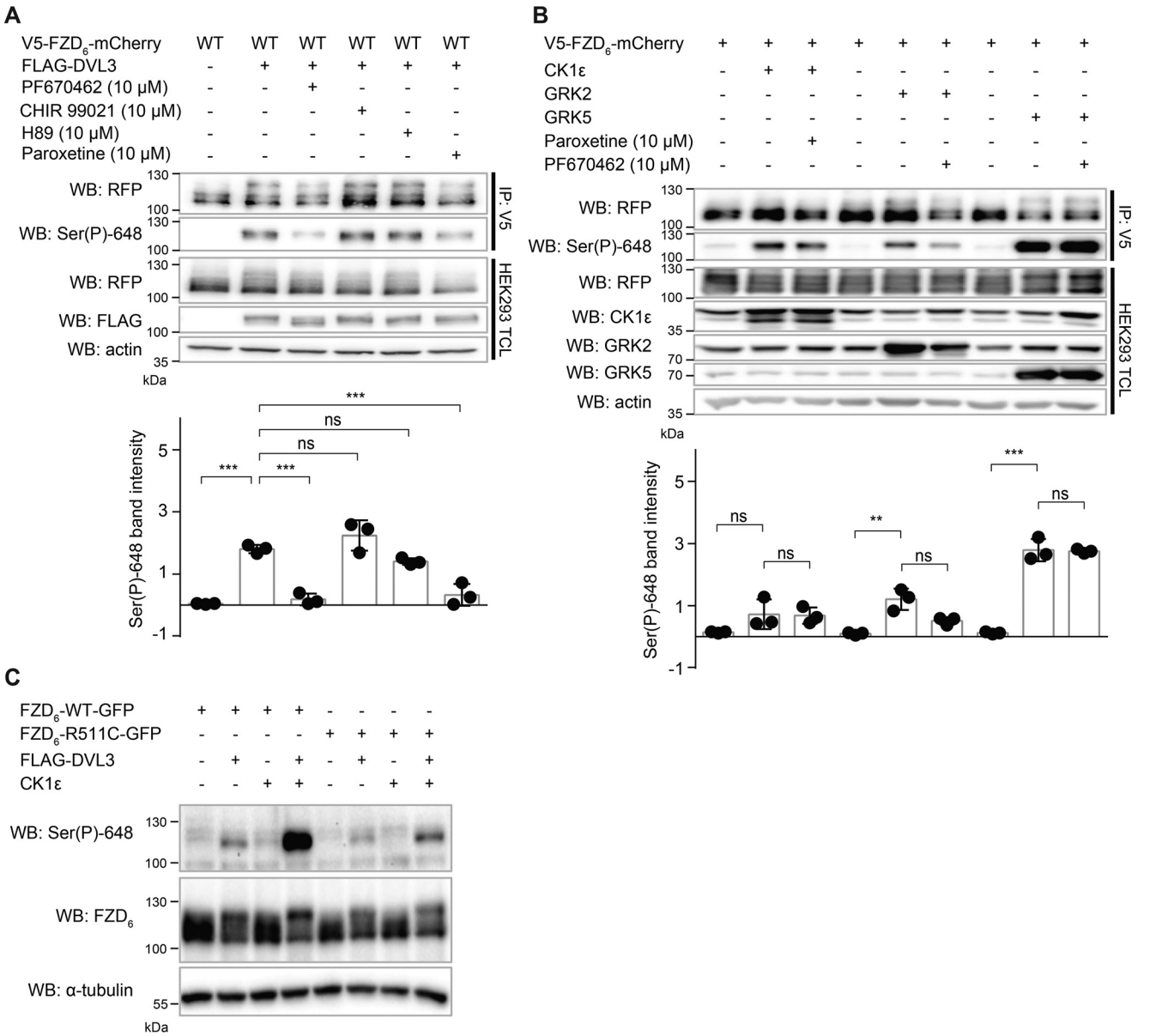

Figure 8. CK1ϵ, GRK2, and GRK5 efficiently phosphorylate Ser(P)-648 FZD$_6$. *A*, HEK293 cells transfected with WT V5-FZD$_6$-mCherry in the absence or presence of FLAG-DVL3. Cells were treated with the CK1 inhibitor PF670462 (10 μM; overnight), the GSK3 inhibitor CHIR 99021 (10 μM; overnight), the PKA inhibitor H89 (10 μM; overnight), or the GRK2 inhibitor paroxetine (10 μM; overnight). V5-FZD$_6$-mCherry was precipitated (*IP*) with the anti-V5 antibody. IP samples and total cell lysates (*TCL*) were analyzed using anti-RFP (mCherry), anti-Ser(P)-648, anti-FLAG, and anti-β-actin as a loading control. *B*, HEK293 cells were cotransfected with WT V5-FZD$_6$-mCherry and either no kinase, CK1ϵ, GRK2, or GRK5. Treatment with paroxetine or PF670642 was overnight at 10 μM. Anti-V5 immunoprecipitates were analyzed by immunoblotting with anti-RFP and anti-Ser(P)-648 antibodies. Total cell lysates (*TCL*) were probed for RFP, CK1ϵ, GRK2, GRK5, and β-actin as a loading control. *A* and *B*, the density of Ser(P)-648 –stained bands, measured using ImageJ, was normalized by dividing each value by the average of the whole experiment. Data are presented as a scatter plot; *bars* represent mean and *error bars* represent S.D. of three individual experiments. Selected results of the multiple comparison analysis of all data are presented. Results were analyzed with one-way ANOVA and Tukey's multiple comparisons post hoc test. Significance levels are given as ** ($p < 0.01$), *** ($p < 0.001$), and *ns* (not significant). *C*, HEK293 cells transfected with WT FZD$_6$-GFP or the nail dysplasia mutant FZD$_6$-GFP-R511C in the absence or presence of FLAG-DVL3 and CK1ϵ were lysed and analyzed by immunoblotting using anti-Ser(P)-648 and anti-FZD$_6$ antibodies. Anti-α-tubulin served as a loading control. *WB*, Western blot.

DVL3) does not promote phosphorylation of Ser(P)-648 and FZD$_6$ shift. Fig. 10*C* shows that Abl-mediated phosphorylation of tyrosine 494 in DVL1, implicated to have a positive effect on DVL function in the PCP pathway, was dispensable for the induction of Ser-648 phosphorylation and the overall FZD$_6$ electrophoretic mobility shift. Mutating clusters of positively charged residues important for DVL binding to the phospholipids in the membrane (mutants RRRKA and HKA) neither affected the DVL1-mediated Ser(P)-648 nor the FZD$_6$ shift (Fig. 10, *D* and *E*). Lastly, the deletion of the N-terminally positioned LPDSG motif in the DEP domain (mutant ΔLPDSG) rendered DVL1 unable to induce Ser(P)-648 or FZD$_6$ shift (Fig. 10*F*). In all our experiments, the electrophoretic mobility shift of FZD$_6$ was accompanied by the phosphorylation of FZD$_6$ at Ser-648 (and vice versa), suggesting that the two events are interconnected.

In summary, our data using DVL mutants show that the DVL-induced hyperphosphorylation of FZD$_6$, including

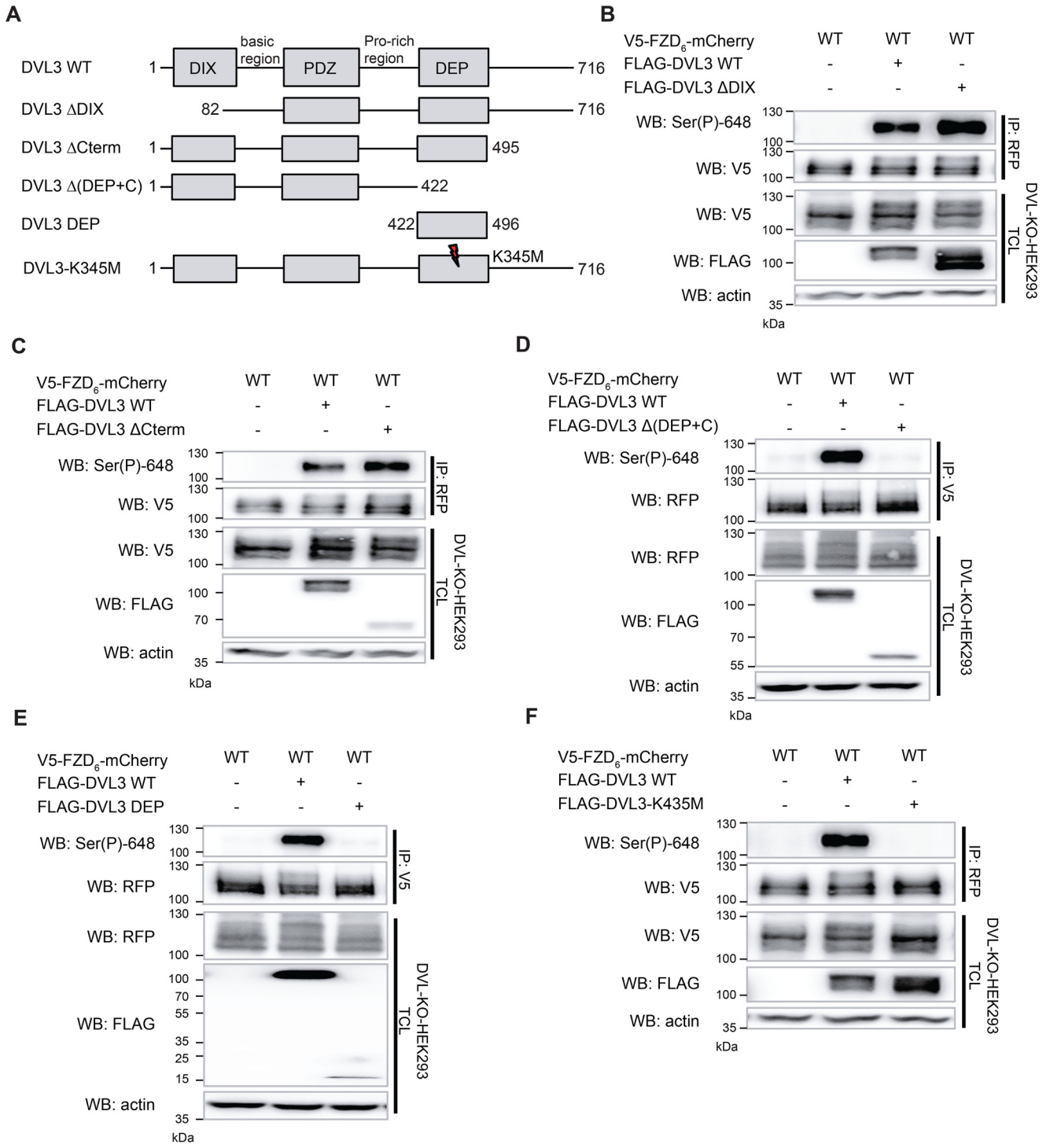

Figure 9. The DEP domain and DVL–FZD interaction are essential to mediate phosphorylation of FZD$_6$ at Ser-648. *A*, schematic depiction of DVL3 constructs used in *B–F*. For details, see the text. *B–F*, DVL-KO-HEK293 cells expressing WT V5-FZD$_6$-mCherry either alone or together with FLAG-DVL3 or one of the FLAG-DVL3 mutants listed above. Cell lysates were precipitated using anti-V5 or anti-RFP. IP and total cell lysate (*TCL*) were analyzed by immunoblotting and probed with anti-Ser(P)-648, anti-RFP, anti-FLAG, and anti-V5 antibodies. Anti-β-actin served as a loading control. Quantification of the Ser(P)-648 FZD$_6$ signal from three independent experiments for each condition is shown in Fig. S4. *WB*, Western blot.

Ser(P)-648, requires (i) the recruitment of DVL to FZD, (ii) DVL-CK1 binding, and (iii) an intact N-terminal LPDSG motif of the DEP domain. Conversely, FZD hyperphosphorylation is neither dependent on the DIX domain of DVL nor on the ability of DVL DEP to be attached to the membrane or to be phosphorylated by Abl.

Localization of Ser(P)-648 FZD$_6$ in human fallopian tube epithelium

Despite the detailed mechanisms that we have identified leading to the DVL- and CK1-dependent phosphorylation of FZD$_6$, its role for cell surface expression of the receptor and the full functional role of Ser(P)-648 remain obscure. Although

A

DVL1 mutant	mutations
DVL1(1-502)	none
DVL1-K438M	K438M
DVL1-Y494F	Y494F
DVL1 RRRKA	R464A/R465A/R468A/K469A
DVL1 HKA	H482A/K486A
DVL1 ΔLPDSG	deletion (L424-G428)

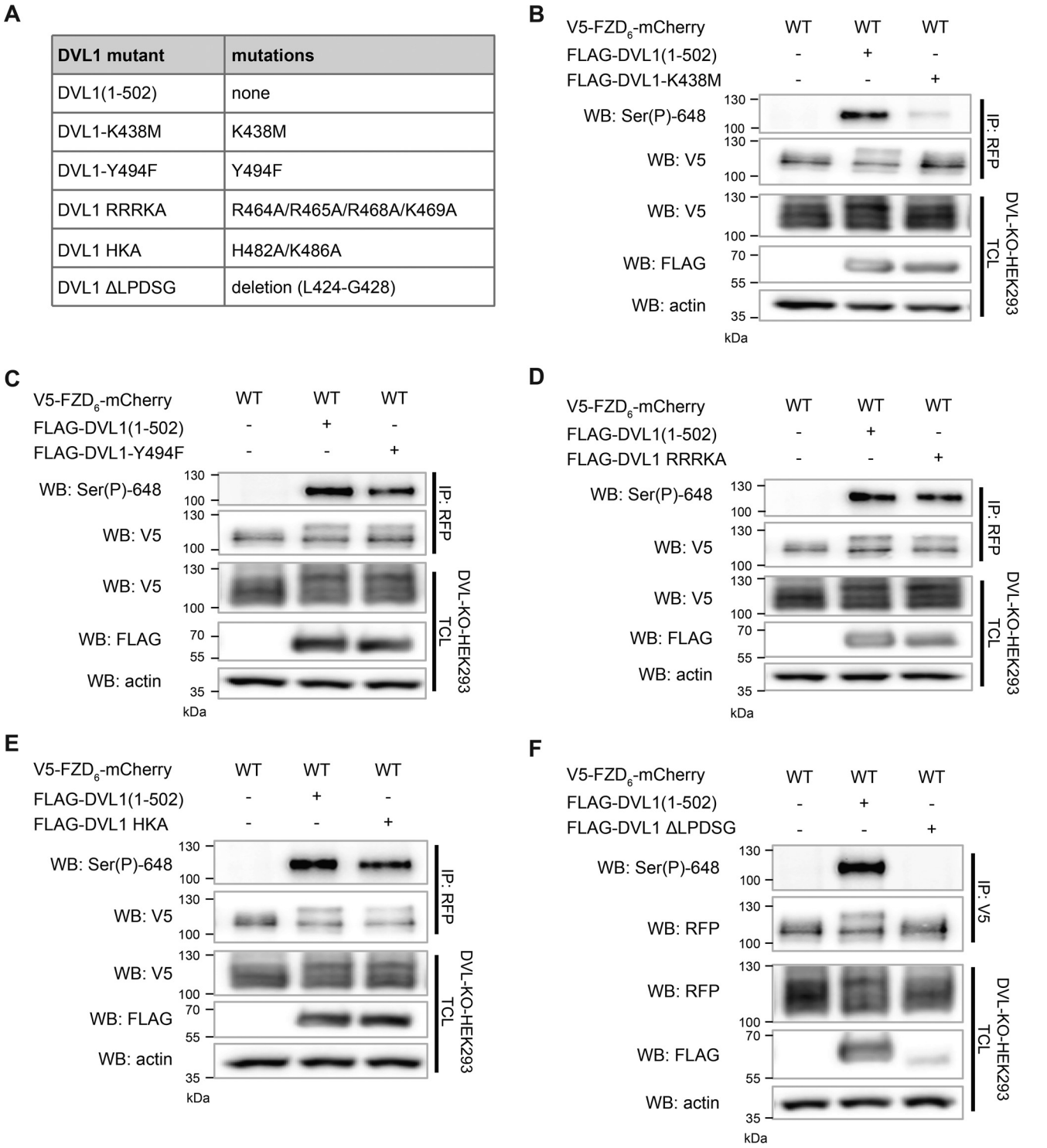

Figure 10. DVL1 DEP mutations differentially affect FZD$_6$ phosphorylation on Ser-648. *A*, table summarizing properties of DVL1 constructs used in *B–F*. *B–F*, WT V5-FZD$_6$-mCherry was overexpressed in DVL-KO-HEK293 cells together with FLAG-DVL1 constructs listed above and immunoprecipitated using an anti-V5 or anti-RFP antibody. Immunoblots show abundance of proteins in the pulldown (*IP*) or total cell lysate (*TCL*) detected by anti-Ser(P)-648, anti-V5, anti-RFP, and anti-FLAG antibodies. Anti-β-actin served as a loading control. Quantification of the Ser(P)-648 FZD$_6$ signal from three independent experiments for each condition is shown in Fig. S5. *WB*, Western blot.

deletion of the CK1ε phosphomotif impairs surface expression, we asked now where Ser(P)-648 FZD$_6$ is localized compared with the total FZD$_6$ pool in human epithelial tissue. According to the protein expression mapping efforts of the Human Protein Atlas (46), FZD$_6$ is widely expressed in epithelial tissues. We focused here on human fallopian tube tissue, which showed a distinct membranous FZD$_6$ immunoreactivity using a polyclonal antibody with a large C-terminal epitope. Parallel staining of adjacent paraffin sections of the same fallopian tube tissue with the anti-Ser(P)-648 FZD$_6$ antiserum revealed a more restricted and polarized immunoreactivity (Fig. 11*A*). Although total FZD$_6$ immunoreactivity was evenly distributed in the

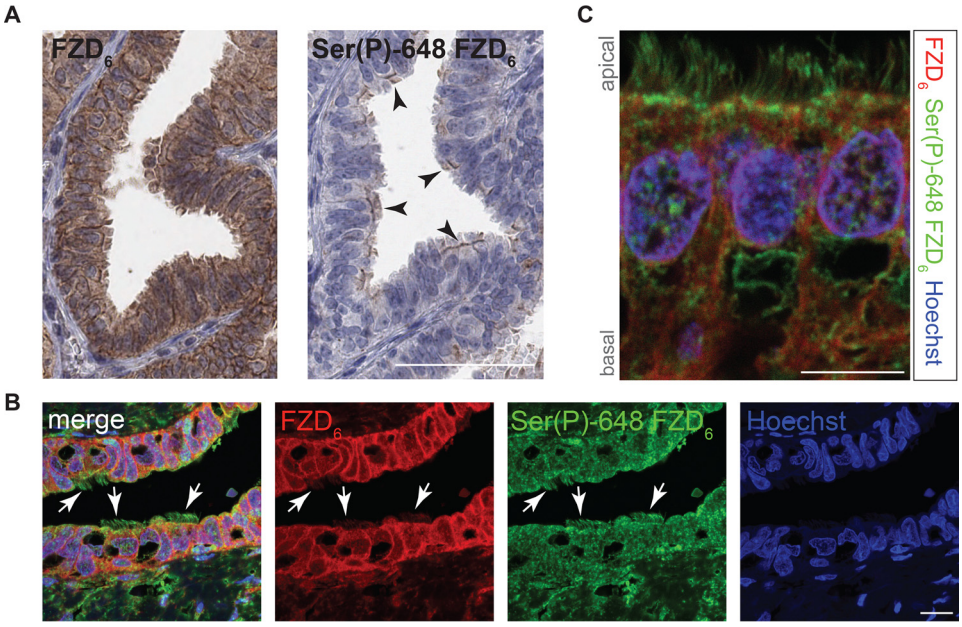

Figure 11. Localization of Ser(P)-648 FZD$_6$ immunoreactivity in human fallopian tube epithelium. *A*, immunohistochemical staining of human fallopian tube tissue with anti-FZD$_6$ and anti-Ser(P)-648 FZD$_6$ antibodies. *Arrows* indicating chromogenic (*brown*) detection of the Ser(P)-648 FZD$_6$ in polarized endothelial cells. *Scale bar*, 60 μm. *B*, immunocytochemical staining of human fallopian tube tissue with anti-FZD$_6$ and anti-Ser(P)-648 FZD$_6$ antibodies indicating a Ser(P)-648 FZD$_6$ distribution in apical parts of endothelial cells and cilia. Nuclei were visualized using Hoechst stain. *Scale bar*, 10 μm. *C*, immunocytochemical staining of human fallopian tube tissue with anti-FZD$_6$ and anti-Ser(P)-648 FZD$_6$ antibodies. *Arrows* point to Ser(P)-648 FZD$_6$ detection in cilia. *Scale bar*, 10 μm.

plasma membrane of all epithelial cells both on the apical and basal side of the cells, Ser(P)-648 FZD$_6$ immunoreactivity was predominantly apical, associated with cilia in a subset of epithelial cells (Fig. 11*B*). Also, double labeling and confocal imaging supported the polarized localization of the phosphorylated FZD$_6$ in fallopian tube epithelial cells (Fig. 11, *B* and *C*).

Discussion

FZDs interact with DVL phosphoproteins in a multimodal fashion, and the interplay has functional but mechanistically poorly understood implications for WNT signaling (4, 5). In addition to DVL, CK1ϵ is a central player of WNT signaling both in β-catenin– dependent and –independent pathways (38, 39, 47–53). Here, we provide evidence that FZD$_6$, CK1ϵ, and DVL cooperate to maintain receptor surface expression and potentially FZD$_6$ polarity in epithelial cells.

Initially, we identified phosphorylation sites in the C terminus of FZD$_6$ by MS/MS in cell lysates exposed to WNT-conditioned medium. Despite enrichment of phosphorylated peptides in cells exposed to WNT-conditioned medium compared with control stimulation, we were at a later time point not able to verify the WNT dependence of the Ser-648 phosphorylation. Because the conditions for the MS/MS experiment did not include overexpression of DVL and CK1 to efficiently enhance FZD phosphorylation, we speculate that Ser-648 FZD$_6$ phosphorylation was a rare event and therefore not efficiently detectable by MS/MS under all conditions.

GRKs represent a family of serine/threonine kinases that regulate GPCR function by direct phosphorylation and by the formation of a ternary complex (3, 54). Here, we have identified GRK2 and GRK5 as two additional kinases able to efficiently phosphorylate FZD$_6$ in the presence of endogenous levels of DVL. Further studies are now required to shed light on the interaction of GRKs and DVL, the requirement of DVL for GRK-mediated FZD phosphorylation, GRK-mediated receptor barcoding regulating desensitization, internalization, and functional selectivity in resemblance to what is known for other GPCRs (1, 3). Interestingly, GRK5 and GRK6 are involved in β-catenin– dependent WNT signaling through phosphorylation of LRP6 (55).

The central tool that we present here is the polyclonal antiserum for detection of Ser-648 phosphorylation of FZD$_6$. We have validated the antibody with regard to phosphorylation state and target selectivity using point mutations of FZD$_6$ and phosphatase treatment of the cell lysates. Furthermore, an efficient and specific signal of the Ser(P)-648 antibody in HEK293 cell lysates is only visible when DVL and kinase are coexpressed, further underlining antibody selectivity. The phosphorylation event on Ser-648 can be seen as a consequence of FZD–DVL interaction. This interaction is intrinsically labile and short-lived and can experimentally be stabilized by chemical cross-linking (11, 56). The antibody provides a new tool to detect the pool of FZD$_6$ that has been in functional contact with DVL and to monitor this transient interaction, which results in Ser-648 phosphorylation. Furthermore, the suitability of the Ser(P)-648 FZD$_6$ antibody for immunohistochemistry could open new possibilities. It remains to be thoroughly validated whether detection of phosphorylated FZDs could present a useful diagnostic tool by screening patient-derived cancer tissue microarrays.

Using the anti-Ser(P)-648 FZD$_6$ antibody, we provide evidence in human fallopian tube epithelium that receptor phosphorylation can contribute to or mirrors cellular asymmetry and polarization of receptor pools. This notion, however, should be taken with a grain of salt because our findings do not distinguish between the possibility that differential localization of Ser(P)-648 FZD$_6$ is the cause or consequence of the phosphorylation event at Ser-648. The experiments with the nail

dysplasia mutant FZD_6-R511C, a mutant that has an intact CK1 phosphorylation motif but shows a mislocalization phenotype with decreased presence at the cell surface (30), suggest that Ser(P)-648 on FZD_6 could mark FZD_6 at the cell surface.

It should also be underlined that receptor-overexpressing HEK293 cells apparently are not a suitable model to mimic receptor distribution in "real" cells such as fallopian epithelial cells. Yet undefined mechanisms appear to be in action to sort subpopulations of receptor pools in a delicate manner, mechanisms that are most likely not present or overridden by receptor overexpression in HEK293 cells. In contrast, the observed changes in receptor surface expression upon single, dual, and triple serine mutation of the CK1-targetd FZD_6 motif underline that FZD_6 phosphorylation is important for efficient membrane embedding or for stabilization of the membrane-expressed receptor pool. In the human fallopian epithelium, it was remarkable that distinct Ser(P) FZD_6 expression was observed only in ciliated cells.

Previously, it was suggested that differential sorting of PCP proteins such as Vangl2 and FZD_6 could contribute to a polarized expression pattern in asymmetric cells (57). Our findings indicate now that receptor phosphorylation could play a complementary role in sorting proteins in a polarized manner in asymmetric cells, providing novel means of cellular polarization by posttranslational modification.

The overall importance of FZD phosphorylation is not yet understood. We have pinpointed a novel mechanism of FZD_6 phosphorylation through CK1 and DVL or GRK2/5 with implications for receptor polarization and cell surface expression. Despite the fact that the C termini across the Class F receptors are poorly conserved, consensus sites of various Ser/Thr kinases are frequent (33), especially when it comes to the closely related FZD_3 and FZD_6, which present the longest C termini in Class F receptors. Thus, CK1-mediated or, more generally speaking, Ser/Thr kinase-mediated phosphorylation of the C termini of FZDs could represent a new concept for FZD regulation and cellular polarization. In support of our findings, previous studies have identified a role of DVL in phosphorylation of FZD_3 with functional implications for receptor hyperphosphorylation, surface expression, and signaling (17, 19). In those studies, the DVL-mediated phosphorylation of FZD_3 evoked a negative feedback on receptor function.

Given the recent information of arrestin barcodes of phosphorylated GPCRs (36), it will be interesting to follow up on our findings by investigating putative arrestin interaction with phosphorylated FZD_6. Although previous findings suggest that DVL bridges FZD–arrestin interaction (58), the DVL-assisted phosphorylation of FZD could play a role in direct arrestin binding to FZDs, resembling the well established GPCR–arrestin interaction (3). Functionally, previous publications point at a central role of arrestins in the regulation of β-catenin– dependent and –independent signaling, and thus, Ser/Thr phosphorylation of FZDs could play an important part in the modulation of WNT signaling (49, 50, 58, 59). Further experiments are needed to better understand the divergent functions of FZD and particularly FZD_6 phosphorylation with regard to polarity, signal specification, desensitization, and arrestin and DVL interaction.

Experimental procedures

Cell culture, transfection, and treatments

WT HEK293 or DVL-KO-HEK293 cells (ATCC) were cultured and transfected as described previously (60). Treatments were done 24 h after transfection using the following agents: PF670462 (sc-204180A, Santa Cruz Biotechnology), CHIR 99021 (1386, Axon Medchem), H89 (B1427, Sigma-Aldrich), paroxetine (PHR1804, Sigma-Aldrich), phorbol 12,13-dibutyrate (P1269, Sigma-Aldrich), dithiobis(succinimidyl propionate) (D3669, Sigma-Aldrich), or the diluent (DMSO) in nontreated samples. Treatment with control, WNT-3A–, or WNT-5A– containing conditioned medium produced in L cells (ATCC) was done at a ratio 1:4 in the standard Dulbecco's modified Eagle's medium used for propagating the HEK293 cells.

DNA constructs

Human FZD_6-GFP (pAcGFP1-N1); human CK1ϵ (pcDNA3); FLAG-DVL1 (pcDNA3); FLAG-DVL3 (pcDNA3.1); and DVL3 ΔDIX, DVL3 ΔC-term, DVL3 Δ(DEP+C), GRK2, and GRK5 (pRK5) were kind gifts from Niklas Dahl, Lukas Trantirek, Madelon Maurice, Randall Moon, and Robert J. Lefkowitz, respectively. FLAG-DVL2 was from Addgene (24802). All FZD_6 mutants used in this study were created in the background of the human V5-FZD_6-mCherry construct (N terminus, V5; C terminus, mCherry; Fig. 2*B*) using the QuikChange site-directed mutagenesis kit (Agilent) according to the manufacturer's instruction, verified by sequencing, and characterized with regard to expression and localization. Primers were as follows: FZD_6-S645A forward primer, 5′-GCAGGCAGTGTATCTGAAGCTGCGCGGAGTGAAGGAAGG-3′; FZD_6-S645A reverse primer, 5′-CCTTCCTTCACTCCGCGCAGCTTCAGATACACTGCCTGC-3′; FZD_6-S645E forward primer, 5′-GCAGGCAGTGTATCTGAAGAGGCGCGGAGTGAAGGAAGG-3′; FZD_6-S645E reverse primer, 5′-CCTTCCTTCACTCCGCGCCTCTTCAGATACACTGCCTGC-3′; FZD_6-S648A forward primer, 5′-GTATCTGAAAGTGCGCGGGCTGAAGGAAGGATTAGTCC-3′; and FZD_6-S648A reverse primer, 5′-GGACTAATCCTTCCTTCAGCCCGCGCACTTTCAGATAC-3′. The FZD_6-S645A/S648A double mutant and the FZD_6-S643A/S645A/S648A and FZD_6-S648A/S653A/S656A triple mutants were created in the background of the V5-FZD_6-S648A-mCherry construct using the following primers: FZD_6-S645A/S648A forward primer, 5′-GGCAGTGTATCTGAAGCTGCGCGGGCTGAAGG-3′; FZD_6-S645A/S648A reverse primer, 5′-CCTTCAGCCCGCGCAGCTTCAGATACACTGCC-3′; FZD_6-S643S/S645A/S648A forward primer, 5′-GGCCAGGCAGTGTAGCTGAAGCTGCGCGGGCTGAAGG-3′; FZD_6-S643S/S645A/S648A reverse primer, 5′-CCTTCAGCCCGCGCAGCTTCAGCTACACTGCCTGGCC-3′; FZD_6-S648A/S653A/S656A forward primer, 5′-TGCGCGGGCTGAAGGAAGGATTGCTCCAAAGGCTGATATTACTGACACTGGCC-3′; and FZD_6-S648A/S653A/S656A reverse primer, 5′-GGCCAGTGTCAGTAATATCAGCCTTTGGAGCAATCCTTCCTTCAGCCCGCGCA-3′. In the same way, the mutant DVL3-K435M was created in the background of the FLAG-DVL3 construct (pcDNA3.1; N terminus, FLAG) using the following primers: DVL3-K435M forward primer,

5′-GTCCGTGACCGCATGTGGCTCATGATTACCATCCCT-AATGCTTTC-3′; and DVL3-K435M reverse primer, 5′-GAAAGCATTAGGGATGGTAATCATGAGCCACATGCG-GTCACGGAC-3′. FZD_4 and FLAG-DVL1 constructs are described elsewhere (11, 45).

Immunoprecipitation (IP), deglycosylation, and dephosphorylation assay

The immunoprecipitation assay was carried out as described previously (38) using anti-V5 (mouse; R960-CUS, Thermo Fisher Scientific) or anti-RFP (rat; 5F8, Chromotek) antibody for pulldown. For the deglycosylation assay, immunoprecipitated samples were incubated overnight at 37 °C in lysis buffer with 1% β-mercaptoethanol and 2 units of *N*-glycosidase F (N-gF; 11365169001, Roche Applied Science). For the dephosphorylation assay, immunoprecipitated samples were incubated for 1 h at 37 °C in CIP buffer (100 mM NaCl, 50 mM Tris-Cl, 10 mM $MgCl_2$, 1 mM DTT, pH 7.9) with EDTA-free protease inhibitor mixture (04693132001, Roche Applied Science) and 10 units of AP (P8361-5000u, Sigma-Aldrich).

Immunoblotting, immunocytochemistry, and live-cell imaging

Lysates in Laemmli buffer were separated by SDS-PAGE/immunoblotting following standard procedures (38). Primary antibodies used were anti-V5 (mouse; 1:5000; R960-CUS, Thermo Fisher Scientific), anti-FLAG M2 (mouse; 1:2000; F1804, Sigma-Aldrich), anti-CK1ϵ (goat; 1:500; sc-6471, Santa Cruz Biotechnology), anti-RFP (rat; 1:2000; 5F8, Chromotek), anti-GRK2 (rabbit; 1:500; sc-562, Santa Cruz Biotechnology), anti-GRK5 (rabbit; 1:500; sc-565, Santa Cruz Biotechnology), anti-DVL2 (rabbit; 1:1000; cs-3224, Cell Signaling Technology), anti-FZD_6 (rabbit; 1:1000; NBP1-89702, Novus-Bio), anti-α-tubulin (mouse; 1:1000; T6199, Sigma-Aldrich), anti-GAPDH (rabbit; 1:8000; 2118S, Cell Signaling Technology), and anti-β-actin (rabbit; 1:2000; 4970, Cell Signaling Technology). The anti-Ser(P)-648 antibody was raised on a service basis by Moravian Biotechnology: the phosphorylated SESARpSEGRISP peptide was injected into rabbit, serum was affinity-purified, and a fraction binding the aforementioned phosphopeptide was used (dilution for both immunoblotting and immunocytochemistry, 1:500).

For immunocytochemistry, transfected cells were fixed on glass coverslips coated with porcine gelatin and processed as described previously (38) using anti-CK1ϵ (goat; 1:1000; sc-6471, Santa Cruz Biotechnology) and anti-Ser(P)-648 FZD_6 (rabbit; 1:500; Moravian Biotechnology) primary antibodies. For live-cell imaging, cells were seeded in glass-bottom dishes and imaged 24 h after transfection using a Leica TCS SP8 confocal microscope.

LC-MS/MS analysis

After the pulldown using the anti-GFP antibody (rabbit; 20R-GR-011, Fitzgerald), samples were incubated with 10 mM DTT at 56 °C for 45 min. After removal of excess DTT, samples were incubated with 55 mM iodoacetamide at room temperature in darkness for 30 min. The trypsin digestion was performed for 2 h at 40 °C on a Thermomixer (750 rpm; Eppendorf). Digested peptides were extracted using 50% acetonitrile solution with 2.5% formic acid (FA) and concentrated in a SpeedVac concentrator (Eppendorf). An aliquot of a concentrated sample was directly analyzed by LC-MS/MS for protein identification. The rest of the sample was used for phosphopeptide analysis. The sample was diluted with acidified acetonitrile solution (80% acetonitrile and 2% FA). Phosphopeptides were enriched using the Pierce Magnetic Titanium Dioxide Phosphopeptide Enrichment kit (Thermo Fisher Scientific) according to the manufacturer's protocol with slight modifications (samples were mixed with binding solution at a 1:2 ratio before loading, and one additional washing step with binding solution after phosphopeptide capture was implemented). Eluates were concentrated under vacuum and then diluted in 10 μl of 0.1% FA solution before LC-MS/MS analysis. The LC-MS analysis was performed on a nanoACQUITY UPLC (Waters Corp.) coupled to a LTQ-Orbitrap Velos mass spectrometer (Thermo Electron Corporation) equipped with a nanoelectrospray ionization source and installed with a Picotip Emitter (New Objective).

For LC separation, the digested peptides were first enriched on a nanoACQUITY UPLC 2G-V/Mtrap Symmetry C_{18} precolumn (2-cm length, 180-μm inner diameter, and 5-μm particle size) from Waters Corp. and separated using a nanoACQUITY BEH130 C_{18} column (10-cm length, 100-μm inner diameter, and 1.7-μm particle size from Waters Corp.). The separation was achieved with the formation of 92-min gradient containing buffer A (2% acetonitrile in water with 0.1% acetic acid) and buffer B (acetonitrile with 0.1% acetic acid; gradient, 2–5% buffer B in 2 min, 5–25% buffer B in 63 min, 25–60% buffer B in 25 min, 60–99% buffer B in 1 min). The peptides were eluted at a flow rate of 400 nl/min. The eluted peptides were analyzed first in the Fourier transform MS operated in positive and profile mode. The second scan event is an MS/MS scan performed in data-dependent mode to fragment peptides and acquire data in positive and centroid mode. The MS automatically switches between Orbitrap-MS and LTQ-MS/MS acquisition to carry out the MS and MS/MS events. Survey full-scan MS spectra (from m/z 300 to 1700) were acquired in the Orbitrap with resolution $R = 30\,000$ with a target value of $1 \times E6$. The method allowed sequential isolation of a maximum of the 20 most intense ions (depending on signal intensity), which were subjected to collision-induced dissociation fragmentation with an isolation width of 2 Da and a target value of $1 \times E4$ or with a maximum ion time of 100 ms. Target ions already selected for MS/MS were dynamically excluded for 60 s. General MS conditions were electrospray voltage of 1.65 kV, no sheath and auxiliary gas flow, and capillary temperature of 300 °C. Ion selection threshold was 1500 counts for MS/MS with an activation time of 10 ms and activation energy of 35% normalized (also applied for MS/MS). Only doubly and triply charged ions were triggered for tandem MS analysis.

The data were analyzed by Thermo Proteome Discoverer 1.4 and searched against the human UniProt fasta database using Sequest HT. The search parameter settings included trypsin as protease with two miscleavages; oxidation of methionine and phosphorylation of serine, threonine, and tyrosine as dynamic modifications; and carbamidomethylation of cysteine as a static modification. A peptide error tolerance of 10 ppm and fragment tolerance of 0.8 Da were used for peptide identifications with a false discovery rate of 1%. Peptides were validated by

node Percolator, and the phosphopeptides were validated by node PhosphoRs 3.0. The output results were later filtered to yield high-confidence peptides and enable protein grouping. The MS proteomics data have been deposited to the ProteomeXchange Consortium via the PRIDE partner repository (61) with the data set identifier PXD011173.

Cell ELISA

For quantification of cell surface receptor expression, 5×10^4 HEK293 cells were plated in 96-well plates coated with 0.1 mg/ml poly-D-lysine. Cells were transfected with 0.1 μg of the indicated constructs and maintained for an additional 24 h. Cells were then incubated with an anti-V5 antibody (mouse; 1:1000; R960-CUS, Thermo Fisher Scientific) in 1% BSA in PBS for 1 h at 4 °C. Following incubation, cells were washed five times with 0.5% BSA in PBS and probed with an horseradish peroxidase–conjugated goat anti-mouse antibody (1:4000; 31430, Thermo Fisher Scientific) in 1% BSA in PBS for 1 h at 4 °C. The cells were washed five times with 0.5% BSA in PBS, and 100 μl of the peroxidase substrate 3,3′,5,5′-tetramethylbenzidine (T8665, Sigma-Aldrich) was added (30 min at room temperature). After acidification with 100 μl of 2 M HCl, the yellow color was read at 450 nm using a POLARstar Omega plate reader (BMG LABTECH).

Human tissue samples and generation of tissue microarrays

The use of Human Protein Atlas (HPA) tissue was covered by the HPA ethical permit (EPN Uppsala, Sweden, 2002/577, 2005/338, 2011/473) following the Declaration of Helsinki principles. Tissue was acquired from the archives at the Department of Pathology of Uppsala University Hospital. In brief, formalin-fixed and paraffin-embedded tissue samples were collected based on hematoxylin- and eosin-stained tissue sections showing representative normal histology, quality-controlled by a certified pathologist. Tissue was sectioned in 4-μm-thick sections using waterfall microtomes (Microm HM 355S, Thermo Fisher Scientific), dried at room temperature overnight, and baked at 50 °C for 12–24 h prior to immunohistochemical staining.

Immunohistochemistry

Tissue sections were deparaffinized in xylene, hydrated in graded alcohols, and blocked for endogenous peroxidase in 0.3% hydrogen peroxide diluted in 95% ethanol. For antigen retrieval, a Decloaking Chamber® (Biocare Medical) was used. Slides were immersed and boiled in citrate buffer, pH 6 (Lab Vision), for 4 min at 125 °C and then allowed to cool to 90 °C (the whole cycle was ~40 min). Automated immunohistochemistry was performed using an Autostainer® 480 instrument (Thermo Fischer Scientific). The primary anti-FZD_6 (rabbit; 1:300; HPA017991, Human Protein Atlas project–Atlas Antibodies AB) and the anti-Ser(P)-648 FZD_6 (rabbit; 1:200; Moravian Biotechnology) were diluted in UltraAb Diluent (Thermo Fisher Scientific) followed by incubation for 30 min at room temperature. The slides were further incubated with the secondary reagent anti-rabbit/mouse horseradish peroxidase-conjugated UltraVision (Thermo Fischer Scientific) for 30 min at room temperature and developed for 10 min using diaminobenzidine Quanto (Thermo Fisher Scientific) as chromogen. All incubations were followed by a rinse in Wash Buffer (Thermo Fisher Scientific) two times for 5 min. Slides were counterstained in Mayer's hematoxylin (Histolab) and coverslipped using Pertex® (Histolab) as mounting medium. The stained slides were dried in oven overnight and digitalized using Scanscope AT2 (Aperio) using a 20× objective.

Immunofluorescence

Anti-FZD_6 and anti-Ser(P)-648 FZD_6 immunoreactivity were visualized using a sequential tyramide signal amplification (PerkinElmer Life Sciences) protocol with an intermediate antibody elution step. Staining was performed in a BOND-RX automated stainer (Leica Biosystems). Slides were dewaxed (Bond Dewax Solution; 72 °C; Leica Biosystems) followed by a heat-induced epitope retrieval step (HIER1 citrate buffer, pH 6.0; 20 min at 100 °C; Leica Biosystems). Endogenous peroxidase activity was blocked with Novocastra Peroxidase Block (RE7171, Leica Biosystems). Samples were sequentially stained with anti-FZD_6 (rabbit; 1:250; HPA017991, Human Protein Atlas project–Atlas Antibodies AB) followed by anti-Ser(P)-648 FZD_6 (rabbit; 1:500; Moravian Biotechnology) and vice versa. Samples were incubated with the first primary antibody for 4 h (2×2 h at room temperature), washed, treated with Post Primary Block before incubation with the horseradish peroxidase polymer detection system (Novacastra Novolink, Leica Biosystems). After several washes, fluorescein-labeled tyramide in amplification diluent (1:100; PerkinElmer Life Sciences) was applied. Tissue-bound primary antibodies and polymer were eluted using a short antigen retrieval step (HIER1; 10 min at 100 °C; Leica Biosystems). For the second primary antibody, the same protocol based on Cy5-labeled tyramide was used. Nuclei were visualized using Hoechst (1:10,000), and lipofuscin autofluorescence in the tissue was quenched with lipophilic Sudan Black B solution (1% (w/v) in 70% ethanol; Sigma-Aldrich) for 5 min. All pictures were taken with a Zeiss LSM880 confocal microscope.

Statistical analysis

All immunoblot experiments are representative of $n = 3$. Statistical and graphical analyses were done using GraphPad Prism 6 software. Quantification of the Western blots was performed by ImageJ software. Briefly, the density of each Ser(P)-648–stained band (Figs. 2*C*; 3, *B* and *D*; 5*B*; 6*A*; 7*B*; 8, *A* and *B*; 9, *B–F*; and 10, *B–F*) was measured and normalized by dividing the value by the average of the whole experiment. Normalized values were plotted as a scatter plot, and bars represent mean ± S.D. of three independent experiments. Differences among the groups were analyzed by one-way ANOVA with Tukey's multiple comparisons post hoc test. Significance levels are given as follows: *, $p < 0.05$; **, $p < 0.01$; and ***, $p < 0.001$. For analyzing cell ELISA data, the basal fluorescence detected in pcDNA-transfected HEK293 cells was subtracted from all data, and mean values were normalized to WT FZD_6 surface expression. Differences among the groups were analyzed by two-tailed *t* test or one-way ANOVA with Dunnett's multiple comparisons post hoc test. Significance levels are given as follows: *, $p < 0.05$; **, $p < 0.01$; and ***, $p < 0.001$. All data points represent normalized values, each performed in triplicates, and values

were plotted as a scatter plot. Bars represent mean ± S.D. of four to five independent experiments.

Author contributions—K. S., J. V., O. B., V. B., and G. S. conceptualization; K. S., J. V., O. B., V. B., and G. S. data curation; K. S., M. K.-J., T. G., V. M. D., R. S. G., Z. Z., and J. M. formal analysis; K. S., M. K.-J., O. B., and V. B. validation; K. S., M. K.-J., T. G., J. V., V. M. D., O. B., R. S. G., Z. Z., J. M., C. L., V. B., and G. S. investigation; K. S., M. K.-J., J. V., O. B., V. B., and G. S. visualization; K. S., M. K.-J., V. M. D., J. H., O. B., Z. Z., J. M., C. L., V. B., and G. S. methodology; K. S., M. K.-J., J. V., O. B., V. B., and G. S. writing-original draft; K. S., M. K.-J., J. V., O. B., V. B., and G. S. writing-review and editing; M. K.-J., J. V., O. B., V. B., and G. S. funding acquisition; J. V., V. M. D., O. B., J. M., C. L., V. B., and G. S. resources; J. V., J. H., O. B., V. B., and G. S. supervision; J. V., O. B., V. B., and G. S. project administration.

Acknowledgments—We thank Lukas Trantirek, Niklas Dahl, Madelon Maurice, Randall Moon, and Robert J Lefkowitz for providing plasmids. Czech Infrastructure for Integrative Structural Biology Research Infrastructure Project LM2015043 funded by the Ministry of Education, Youth and Sports of the Czech Republic is gratefully acknowledged for the financial support of the LC-MS/MS measurements at the Central European Institute of Technology Proteomics Core Facility.

References

1. Tobin, A. B. (2008) G-protein-coupled receptor phosphorylation: where, when and by whom. *Br. J. Pharmacol.* **153,** Suppl. 1, S167–S176 CrossRef Medline
2. Yang, Z., Yang, F., Zhang, D., Liu, Z., Lin, A., Liu, C., Xiao, P., Yu, X., and Sun, J. P. (2017) Phosphorylation of G protein-coupled receptors: from the barcode hypothesis to the flute model. *Mol. Pharmacol.* **92,** 201–210 CrossRef Medline
3. Reiter, E., and Lefkowitz, R. J. (2006) GRKs and β-arrestins: roles in receptor silencing, trafficking and signaling. *Trends Endocrinol. Metab.* **17,** 159–165 CrossRef Medline
4. Gao, C., and Chen, Y. G. (2010) Dishevelled: the hub of Wnt signaling. *Cell. Signal.* **22,** 717–727 CrossRef Medline
5. Mlodzik, M. (2016) The Dishevelled protein family: still rather a mystery after over 20 years of molecular studies. *Curr. Top. Dev. Biol.* **117,** 75–91 CrossRef Medline
6. Gammons, M. V., Rutherford, T. J., Steinhart, Z., Angers, S., and Bienz, M. (2016) Essential role of the Dishevelled DEP domain in a Wnt-dependent human-cell-based complementation assay. *J. Cell Sci.* **129,** 3892–3902 CrossRef Medline
7. Gammons, M. V., Renko, M., Johnson, C. M., Rutherford, T. J., and Bienz, M. (2016) Wnt signalosome assembly by DEP domain swapping of Dishevelled. *Mol. Cell* **64,** 92–104 CrossRef Medline
8. Umbhauer, M., Djiane, A., Goisset, C., Penzo-Méndez, A., Riou, J. F., Boucaut, J. C., and Shi, D. L. (2000) The C-terminal cytoplasmic Lys-Thr-X-X-X-Trp motif in frizzled receptors mediates Wnt/β-catenin signalling. *EMBO J.* **19,** 4944–4954 CrossRef Medline
9. Tauriello, D. V., Jordens, I., Kirchner, K., Slootstra, J. W., Kruitwagen, T., Bouwman, B. A., Noutsou, M., Rüdiger, S. G., Schwamborn, K., Schambony, A., and Maurice, M. M. (2012) Wnt/β-catenin signaling requires interaction of the Dishevelled DEP domain and C terminus with a discontinuous motif in Frizzled. *Proc. Natl. Acad. Sci. U.S.A.* **109,** E812–E820 CrossRef Medline
10. Pau, M. S., Gao, S., Malbon, C. C., Wang, H. Y., and Bertalovitz, A. C. (2015) The intracellular loop 2 F328S Frizzled-4 mutation implicated in familial exudative vitreoretinopathy impairs Dishevelled recruitment. *J. Mol. Signal.* **10,** 5 CrossRef Medline
11. Strakova, K., Matricon, P., Yokota, C., Arthofer, E., Bernatik, O., Rodriguez, D., Arenas, E., Carlsson, J., Bryja, V., and Schulte, G. (2017) The tyrosine Y250(2.39) in Frizzled 4 defines a conserved motif important for structural integrity of the receptor and recruitment of Dishevelled. *Cell. Signal.* **38,** 85–96 CrossRef Medline
12. Dijksterhuis, J. P., Petersen, J., and Schulte, G. (2014) WNT/Frizzled signaling: receptor-ligand selectivity with focus on FZD-G protein signaling and its physiological relevance. *Br. J. Pharmacol.* **171,** 1195–1209 CrossRef Medline
13. Schulte, G., and Bryja, V. (2007) The Frizzled family of unconventional G-protein-coupled receptors. *Trends Pharmacol. Sci.* **28,** 518–525 CrossRef Medline
14. Schulte, G. (2010) International Union of Basic and Clinical Pharmacology. LXXX. The class Frizzled receptors. *Pharmacol. Rev.* **62,** 632–667 CrossRef Medline
15. Koval, A., Purvanov, V., Egger-Adam, D., and Katanaev, V. L. (2011) Yellow submarine of the Wnt/Frizzled signaling: submerging from the G protein harbor to the targets. *Biochem. Pharmacol.* **82,** 1311–1319 CrossRef Medline
16. Djiane, A., Yogev, S., and Mlodzik, M. (2005) The apical determinants aPKC and dPatj regulate Frizzled-dependent planar cell polarity in the *Drosophila* eye. *Cell* **121,** 621–631 CrossRef Medline
17. Shafer, B., Onishi, K., Lo, C., Colakoglu, G., and Zou, Y. (2011) Vangl2 promotes Wnt/planar cell polarity-like signaling by antagonizing Dvl1-mediated feedback inhibition in growth cone guidance. *Dev. Cell* **20,** 177–191 CrossRef Medline
18. Yanfeng, W. A., Tan, C., Fagan, R. J., and Klein, P. S. (2006) Phosphorylation of frizzled-3. *J. Biol. Chem.* **281,** 11603–11609 CrossRef Medline
19. Onishi, K., Shafer, B., Lo, C., Tissir, F., Goffinet, A. M., and Zou, Y. (2013) Antagonistic functions of Dishevelleds regulate Frizzled3 endocytosis via filopodia tips in Wnt-mediated growth cone guidance. *J. Neurosci.* **33,** 19071–19085 CrossRef Medline
20. Regard, J. B., Sato, I. T., and Coughlin, S. R. (2008) Anatomical profiling of G protein-coupled receptor expression. *Cell* **135,** 561–571 CrossRef Medline
21. Corda, G., and Sala, A. (2017) Non-canonical WNT/PCP signalling in cancer: Fzd6 takes centre stage. *Oncogenesis* **6,** e364 CrossRef Medline
22. Kilander, M. B., Petersen, J., Andressen, K. W., Ganji, R. S., Levy, F. O., Schuster, J., Dahl, N., Bryja, V., and Schulte, G. (2014) Disheveled regulates precoupling of heterotrimeric G proteins to Frizzled 6. *FASEB J.* **28,** 2293–2305 CrossRef Medline
23. Kilander, M. B., Dahlström, J., and Schulte, G. (2014) Assessment of Frizzled 6 membrane mobility by FRAP supports G protein coupling and reveals WNT-Frizzled selectivity. *Cell. Signal.* **26,** 1943–1949 CrossRef Medline
24. Wang, Y., Guo, N., and Nathans, J. (2006) The role of Frizzled3 and Frizzled6 in neural tube closure and in the planar polarity of inner-ear sensory hair cells. *J. Neurosci.* **26,** 2147–2156 CrossRef Medline
25. Guo, N., Hawkins, C., and Nathans, J. (2004) Frizzled6 controls hair patterning in mice. *Proc. Natl. Acad. Sci. U.S.A.* **101,** 9277–9281 CrossRef Medline
26. Golan, T., Yaniv, A., Bafico, A., Liu, G., and Gazit, A. (2004) The human Frizzled 6 (HFz6) acts as a negative regulator of the canonical Wnt·β-catenin signaling cascade. *J. Biol. Chem.* **279,** 14879–14888 CrossRef Medline
27. Hua, Z. L., Chang, H., Wang, Y., Smallwood, P. M., and Nathans, J. (2014) Partial interchangeability of Fz3 and Fz6 in tissue polarity signaling for epithelial orientation and axon growth and guidance. *Development* **141,** 3944–3954 CrossRef Medline
28. Cui, C. Y., Klar, J., Georgii-Heming, P., Fröjmark, A. S., Baig, S. M., Schlessinger, D., and Dahl, N. (2013) Frizzled6 deficiency disrupts the differentiation process of nail development. *J. Invest. Dermatol.* **133,** 1990–1997 CrossRef Medline
29. Naz, G., Pasternack, S. M., Perrin, C., Mattheisen, M., Refke, M., Khan, S., Gul, A., Simons, M., Ahmad, W., and Betz, R. C. (2012) FZD6 encoding the Wnt receptor frizzled 6 is mutated in autosomal-recessive nail dysplasia. *Br. J. Dermatol.* **166,** 1088–1094 CrossRef Medline
30. Fröjmark, A. S., Schuster, J., Sobol, M., Entesarian, M., Kilander, M. B. C., Gabrikova, D., Nawaz, S., Baig, S. M., Schulte, G., Klar, J., and Dahl, N.

(2011) Mutations in Frizzled 6 cause isolated autosomal-recessive nail dysplasia. *Am. J. Hum. Genet.* **88,** 852–860 CrossRef Medline
31. Wang, Y., Thekdi, N., Smallwood, P. M., Macke, J. P., and Nathans, J. (2002) Frizzled-3 is required for the development of major fiber tracts in the rostral CNS. *J. Neurosci.* **22,** 8563–8573 CrossRef Medline
32. Wang, Y., Chang, H., Rattner, A., and Nathans, J. (2016) Frizzled receptors in development and disease. *Curr. Top. Dev. Biol.* **117,** 113–139 CrossRef Medline
33. Schulte, G. (2010) Molecular pharmacology of Frizzleds—with implications for possible therapy, in *GPCR Molecular Pharmacology and Drug Targeting* (Gilchrist, A., ed) John Wiley and Sons, Hoboken, NJ
34. Balla, S., Thapar, V., Verma, S., Luong, T., Faghri, T., Huang, C. H., Rajasekaran, S., del Campo, J. J., Shinn, J. H., Mohler, W. A., Maciejewski, M. W., Gryk, M. R., Piccirillo, B., Schiller, S. R., and Schiller, M. R. (2006) Minimotif Miner: a tool for investigating protein function. *Nat. Methods* **3,** 175–177 CrossRef Medline
35. Petersen, J., Wright, S. C., Rodríguez, D., Matricon, P., Lahav, N., Vromen, A., Friedler, A., Strömqvist, J., Wennmalm, S., Carlsson, J., and Schulte, G. (2017) Agonist-induced dimer dissociation as a macromolecular step in G protein-coupled receptor signaling. *Nat. Commun.* **8,** 226 CrossRef Medline
36. Zhou, X. E., He, Y., de Waal, P. W., Gao, X., Kang, Y., Van Eps, N., Yin, Y., Pal, K., Goswami, D., White, T. A., Barty, A., Latorraca, N. R., Chapman, H. N., Hubbell, W. L., Dror, R. O., *et al.* (2017) Identification of phosphorylation codes for arrestin recruitment by G protein-coupled receptors. *Cell* **170,** 457–469.e13 CrossRef Medline
37. Cong, F., Schweizer, L., and Varmus, H. (2004) Casein kinase Iε modulates the signaling specificities of dishevelled. *Mol. Cell. Biol.* **24,** 2000–2011 CrossRef Medline
38. Bernatik, O., Ganji, R. S., Dijksterhuis, J. P., Konik, P., Cervenka, I., Polonio, T., Krejci, P., Schulte, G., and Bryja, V. (2011) Sequential activation and inactivation of Dishevelled in the Wnt/β-catenin pathway by casein kinases. *J. Biol. Chem.* **286,** 10396–10410 CrossRef Medline
39. Bryja, V., Schulte, G., Rawal, N., Grahn, A., and Arenas, E. (2007) Wnt-5a induces Dishevelled phosphorylation and dopaminergic differentiation via a CK1-dependent mechanism. *J. Cell Sci.* **120,** 586–595 CrossRef Medline
40. Cervenka, I., Valnohova, J., Bernatik, O., Harnos, J., Radsetoulal, M., Sedova, K., Hanakova, K., Potesil, D., Sedlackova, M., Salasova, A., Steinhart, Z., Angers, S., Schulte, G., Hampl, A., Zdrahal, Z., *et al.* (2016) Dishevelled is a NEK2 kinase substrate controlling dynamics of centrosomal linker proteins. *Proc. Natl. Acad. Sci. U.S.A.* **113,** 9304–9309 CrossRef Medline
41. Schwarz-Romond, T., Fiedler, M., Shibata, N., Butler, P. J., Kikuchi, A., Higuchi, Y., and Bienz, M. (2007) The DIX domain of Dishevelled confers Wnt signaling by dynamic polymerization. *Nat. Struct. Mol. Biol.* **14,** 484–492 CrossRef Medline
42. Fiedler, M., Mendoza-Topaz, C., Rutherford, T. J., Mieszczanek, J., and Bienz, M. (2011) Dishevelled interacts with the DIX domain polymerization interface of Axin to interfere with its function in down-regulating β-catenin. *Proc. Natl. Acad. Sci. U.S.A.* **108,** 1937–1942 CrossRef Medline
43. Axelrod, J. D., Miller, J. R., Shulman, J. M., Moon, R. T., and Perrimon, N. (1998) Differential recruitment of Dishevelled provides signaling specificity in the planar cell polarity and Wingless signaling pathways. *Genes Dev.* **12,** 2610–2622 CrossRef Medline
44. Wong, H. C., Mao, J., Nguyen, J. T., Srinivas, S., Zhang, W., Liu, B., Li, L., Wu, D., and Zheng, J. (2000) Structural basis of the recognition of the dishevelled DEP domain in the Wnt signaling pathway. *Nat. Struct. Biol.* **7,** 1178–1184 CrossRef Medline
45. Paclikova, P., Bernatik, O., Radaszkiewicz, T. W., and Bryja, V. (2017) N-terminal part of Dishevelled DEP domain is required for Wnt/β-catenin signaling in mammalian cells. *Mol. Cell. Biol.* **37,** e00145-17 CrossRef Medline
46. Uhlén, M., Fagerberg, L., Hallström, B. M., Lindskog, C., Oksvold, P., Mardinoglu, A., Sivertsson, Å., Kampf, C., Sjöstedt, E., Asplund, A., Olsson, I., Edlund, K., Lundberg, E., Navani, S., Szigyarto, C. A., *et al.* (2015) Proteomics. Tissue-based map of the human proteome. *Science* **347,** 1260419 CrossRef Medline
47. Strutt, H., Price, M. A., and Strutt, D. (2006) Planar polarity is positively regulated by casein kinase Iε in *Drosophila*. *Curr. Biol.* **16,** 1329–1336 CrossRef Medline
48. Bernatík, O., Šedová, K., Schille, C., Ganji, R. S., Červenka, I., Trantírek, L., Schambony, A., Zdráhal, Z., and Bryja, V. (2014) Functional analysis of dishevelled-3 phosphorylation identifies distinct mechanisms driven by casein kinase 1 and frizzled5. *J. Biol. Chem.* **289,** 23520–23533 CrossRef Medline
49. Bryja, V., Gradl, D., Schambony, A., Arenas, E., and Schulte, G. (2007) β-Arrestin is a necessary component of Wnt/β-catenin signaling *in vitro* and *in vivo*. *Proc. Natl. Acad. Sci. U.S.A.* **104,** 6690–6695 CrossRef Medline
50. Bryja, V., Schambony, A., Cajánek, L., Dominguez, I., Arenas, E., and Schulte, G. (2008) β-Arrestin and casein kinase 1/2 define distinct branches of non-canonical WNT signalling pathways. *EMBO Rep.* **9,** 1244–1250 CrossRef Medline
51. Bryja, V., Schulte, G., and Arenas, E. (2007) Wnt-3a utilizes a novel low dose and rapid pathway that does not require casein kinase 1-mediated phosphorylation of Dvl to activate β-catenin. *Cell. Signal.* **19,** 610–616 CrossRef Medline
52. Kaucká, M., Plevová, K., Pavlová, S., Janovská, P., Mishra, A., Verner, J., Procházková, J., Krejcí, P., Kotasková, J., Ovesná, P., Tichy, B., Brychtová, Y., Doubek, M., Kozubík, A., Mayer, J., *et al.* (2013) The planar cell polarity pathway drives pathogenesis of chronic lymphocytic leukemia by the regulation of B-lymphocyte migration. *Cancer Res.* **73,** 1491–1501 CrossRef Medline
53. Witte, F., Bernatik, O., Kirchner, K., Masek, J., Mahl, A., Krejci, P., Mundlos, S., Schambony, A., Bryja, V., and Stricker, S. (2010) Negative regulation of Wnt signaling mediated by CK1-phosphorylated Dishevelled via Ror2. *FASEB J.* **24,** 2417–2426 CrossRef Medline
54. Komolov, K. E., Du, Y., Duc, N. M., Betz, R. M., Rodrigues, J. P. G. L. M., Leib, R. D., Patra, D., Skiniotis, G., Adams, C. M., Dror, R. O., Chung, K. Y., Kobilka, B. K., and Benovic, J. L. (2017) Structural and functional analysis of a β2-adrenergic receptor complex with GRK5. *Cell* **169,** 407–421.e16 CrossRef Medline
55. Chen, M., Philipp, M., Wang, J., Premont, R. T., Garrison, T. R., Caron, M. G., Lefkowitz, R. J., and Chen, W. (2009) G Protein-coupled receptor kinases phosphorylate LRP6 in the Wnt pathway. *J. Biol. Chem.* **284,** 35040–35048 CrossRef Medline
56. Simons, M., Gault, W. J., Gotthardt, D., Rohatgi, R., Klein, T. J., Shao, Y., Lee, H. J., Wu, A. L., Fang, Y., Satlin, L. M., Dow, J. T., Chen, J., Zheng, J., Boutros, M., and Mlodzik, M. (2009) Electrochemical cues regulate assembly of the Frizzled/Dishevelled complex at the plasma membrane during planar epithelial polarization. *Nat. Cell Biol.* **11,** 286–294 CrossRef Medline
57. Ma, T., Li, B., Wang, R., Lau, P. K., Huang, Y., Jiang, L., Schekman, R., and Guo, Y. (2018) A mechanism for differential sorting of the planar cell polarity proteins Frizzled6 and Vangl2 at the trans-Golgi network. *J. Biol. Chem.* **293,** 8410–8427 CrossRef Medline
58. Chen, W., ten Berge, D., Brown, J., Ahn, S., Hu, L. A., Miller, W. E., Caron, M. G., Barak, L. S., Nusse, R., and Lefkowitz, R. J. (2003) Dishevelled 2 recruits β-arrestin 2 to mediate Wnt5A-stimulated endocytosis of Frizzled 4. *Science* **301,** 1391–1394 CrossRef Medline
59. Schulte, G., Schambony, A., and Bryja, V. (2010) β-Arrestins—scaffolds and signalling elements essential for WNT/Frizzled signalling pathways? *Br. J. Pharmacol.* **159,** 1051–1058 CrossRef Medline
60. Arthofer, E., Hot, B., Petersen, J., Strakova, K., Jäger, S., Grundmann, M., Kostenis, E., Gutkind, J. S., and Schulte, G. (2016) WNT stimulation dissociates a Frizzled 4 inactive-state complex with Gα12/13. *Mol. Pharmacol.* **90,** 447–459 CrossRef Medline
61. Vizcaíno, J. A., Csordas, A., del-Toro, N., Dianes, J. A., Griss, J., Lavidas, I., Mayer, G., Perez-Riverol, Y., Reisinger, F., Ternent, T., Xu, Q. W., Wang, R., and Hermjakob, H. (2016) 2016 update of the PRIDE database and its related tools. *Nucleic Acids Res.* **44,** D447–D456 CrossRef Medline